# Control of CD1d-restricted antigen presentation and inflammation by sphingomyelin

Espen Melum[1,2,*], Xiaojun Jiang[2], Kristi D. Baker[1,3], M. Fatima Macedo[4,5,6], Jürgen Fritsch[7,8], C. Marie Dowds[9], Jing Wang[10], Anne Pharo[2], Arthur Kaser[11], Corey Tan[1,2], Catia S. Pereira[4,5], Samuel L. Kelly[12], Jingjing Duan[12,**], Tom H. Karlsen[2], Mark A. Exley[1], Stefan Schütze[7], Dirk M. Zajonc[10,13], Alfred H. Merrill[12], Edward H. Schuchman[14], Sebastian Zeissig[9,15,16,†], Richard S. Blumberg[1,*,†]

[1]Gastroenterology Division, Department of Medicine, Brigham and Women's Hospital, Harvard Medical School, Boston, USA

[2]Norwegian PSC Research Center, Department of Transplantation Medicine, Division of Surgery, Inflammatory diseases and Transplantation, Oslo University Hospital, Rikshospitalet, and University of Oslo, Oslo, Norway

[3]Department of Oncology, Medical Microbiology and Immunology, University of Alberta, Canada

[4]i3S - Instituto de Investigação e Inovação em Saúde, Universidade do Porto, Portugal

[5]Lysosome and Peroxisome Biology Unit (UniLiPe), IBMC – Instituto de Biologia Molecular e Celular, Universidade do Porto, Porto, Portugal

[6]Department of Medical Sciences, University of Aveiro, Aveiro, Portugal

[7]Institute of Immunology, Christian-Albrechts-University of Kiel, Kiel, Germany

[8]Institute for Clinical Microbiology and Hygiene, University of Regensburg, Regensburg, Germany

[9]Department of Internal Medicine I, University Medical Center Schleswig-Holstein, Christian-Albrechts-University, Kiel, Germany

[10]Division of Immune Regulation, La Jolla Institute for Allergy and Immunology, La Jolla, California, USA

[11]Division of Gastroenterology and Hepatology, Department of Medicine, University of Cambridge, Addenbrooke's Hospital, Cambridge, UK

[12]School of Biology, and the Petit Institute for Bioengineering and Biosciences, Georgia Institute of Technology, Atlanta, Georgia, USA

[13]Department of Internal Medicine, Faculty of Medicine and Health Sciences, Ghent University, Ghent, Belgium

[14]Department of Genetics & Genomic Sciences, Icahn School of Medicine at Mount Sinai, New York, New York, USA

[15]Department of Medicine I, University Medical Center Dresden, Technische Universität (TU) Dresden, Dresden, Germany

[16]Center for Regenerative Therapies Dresden (CRTD), Technische Universität (TU) Dresden, Dresden, Germany

[*]To whom correspondence should be addressed: espen.melum@medisin.uio.no (EM), rsblumberg@bwh.harvard.edu (RSB)

[**]Current address: Human Aging Research Institute, School of Life Sciences, Nanchang University, Nanchang, Jiangxi, China. 330031

[†]These authors share senior authorship

**ABSTRACT**

**Invariant natural killer T (iNKT) cells recognize activating self and microbial lipids presented by CD1d. CD1d can also bind non-activating lipids, such as sphingomyelin. We hypothesized that these serve as endogenous regulators and investigated humans and mice deficient in acid sphingomyelinase (ASM), an enzyme that degrades sphingomyelin. We show that ASM absence in mice leads to diminished CD1d-restricted antigen presentation and iNKT cell selection resulting in decreased iNKT cell levels and resistance to iNKT cell-mediated inflammatory conditions. Defective antigen presentation and decreased iNKT cells are also observed in ASM-deficient humans with Niemann-Pick Disease and ASM activity in healthy humans correlates with iNKT cell phenotype. Pharmacological ASM administration facilitates antigen presentation and restores the levels of iNKT cells in *Asm*$^{-/-}$ mice. Together, these results demonstrate that control of non-agonistic CD1d-associated lipids is critical for iNKT cell development and function *in vivo* and represent a tight link between cellular sphingolipid metabolism and immunity.**

Invariant natural killer T (iNKT) cells are an important lymphocyte population that serves in sensing self and microbial lipids presented by the major histocompatibility complex (MHC) class I-like glycoprotein CD1d[1]. In response to these antigens, iNKT cells rapidly release large arrays of mediators, making them powerful and early modulators of immune pathways[2]. The self-reactivity of iNKT cells is also critical for their development in the thymus[3]. Here, iNKT cells are positively selected by CD1d-bearing thymocytes[4]. While there have been significant efforts to identify CD1d-binding, iNKT cell activating lipids (i.e. lipid antigens[5]), iNKT cell activation is also amenable to negative regulation by CD1d-associated lipids which do not stimulate the iNKT T cell receptor (TCR). As such, iNKT cell activation is anticipated to be influenced by the balance of CD1d-associated antigenic and non-antigenic lipids. However, little is known about the functional relevance of non-antigenic lipids that potentially impede CD1d-restricted iNKT cell activation. Sphingolipids, which are abundantly present in the cell membrane[6], are a major class of CD1d-associated lipids[7,8]. Sphingomyelin, a dominant sphingolipid in mammals, has been reported to be a non-stimulatory CD1d-associated lipid *in vitro*[9], leading us to hypothesize that it may regulate CD1d access to potentially agonistic lipids.

Sphingomyelin is degraded by sphingomyelinases into ceramide and phosphorylcholine[10]. In lysosomes, one of the sites where the exchange and loading of lipids onto CD1d takes place[11], acid sphingomyelinase (ASM) is the primary enzyme responsible for sphingomyelin degradation[12,13]. In light of the non-stimulatory nature of sphingomyelin *in vitro*[9], we sought to understand the consequences of sphingomyelin accumulation on iNKT cell function. To do so, we took advantage of *Asm*$^{-/-}$ mice[14] that develop an age-dependent accumulation of

sphingomyelin and a clinical phenotype resembling ASM-deficiency in humans, known as Niemann-Pick Disease Types A and B (NPD-A and –B), where type A is the more severe form of disease debuting during infancy. We demonstrate that control of the cellular abundance of sphingomyelin by ASM regulates the presentation of endogenous and exogenous lipid antigens by CD1d in thymocytes and dendritic cells (DC) and thus the abundance and activation of iNKT cells. In the absence of ASM in mice, sphingomyelin levels increase in hematopoietic cells resulting in decreased CD1d-restricted antigen presentation, impaired iNKT cell development in the thymus and reduced abundance and activation of iNKT cells – defects that are reversed by the transfer of wildtype bone-marrow or administration of recombinant human (rh)ASM. These observations are extensible to humans with or without NPD and establish ASM, through its control of sphingomyelin levels, as an important regulator of iNKT cells with potential therapeutic implications.

## RESULTS

### ASM is active in the hematopoietic system and required for iNKT cell development

Although it is well established that ASM is expressed in tissues where the clinical phenotypes of NPD-A and –B are most prominent, such as the liver and brain as well as in some hematopoietic cells, such as macrophages[15], little is known about its function in the immune system. Therefore, we first investigated ASM activity and found it to be demonstrable in a variety of parenchymal (colon, liver) and hematopoietic (spleen, thymus and DC) cells with the highest levels in DCs (Fig. 1a), a critical CD1d-expressing antigen presenting cell (APC) in the periphery[16]. Consistent with this being functionally important, flow cytometry (gating strategies in

Supplementary Fig. 1), revealed a dramatic reduction of iNKT cells in the thymus, liver and spleen of adult *Asm*$^{-/-}$ mice (Fig. 1b, 1c and Supplementary Fig. 2a). This was associated with a perturbation in the distribution of the few remaining iNKTs, as shown by decreased relative levels of iNKT cells which expressed CD4 and a relative enrichment in the CD4$^{-}$CD8$^{-}$ (double negative, DN) iNKT cell fraction in the periphery (spleen and liver) (Supplementary Fig. 2b). The reduction in iNKT cell abundance was also associated with a decrease in absolute iNKT cell numbers (Fig. 1d). Furthermore, when PBS57-loaded CD1d tetramer positive cells (i.e. iNKT cells) were excluded there were no changes in the relative abundance of tetramer-negative thymic T cells (Supplementary Fig. 3a) or alterations in the distribution of CD4$^{+}$, CD8$^{+}$, DN or CD4$^{+}$CD8$^{+}$ (double-positive, DP) thymocytes (Supplementary Fig. 3b). In the periphery, tetramer-negative T cells were unaltered in relative abundance in the livers of *Asm*$^{-/-}$ mice and slightly reduced in the spleen of these mice (Supplementary Fig. 3a) in association with minor changes in proportion of CD4$^{+}$, CD8$^{+}$ and DN cells (Supplementary Fig. 3b). We also did not observe changes in the relative abundance of γδ T cells, another type of unconventional T cell, and T regulatory ($T_{reg}$) cells when tetramer positive cells were excluded from the analysis (Supplementary Fig. 3c). To rule out that the reduction in iNKT cells was secondary to a general disturbance of lysosomal function, we investigated mice just after weaning at the age of 2 weeks, when the accumulation of sphingomyelin in parenchymal tissues is known to be minimal[14]. In these young mice, we also observed a reduction in iNKT cells (Fig. 1e). These studies demonstrate that ASM is functionally present in immune tissues and deficiency is associated with a specific alteration of iNKT cell homeostasis.

**ASM is a major regulator of iNKT cell function *in vivo***

To determine whether ASM-deficiency affects iNKT cell function *in vivo*, we examined the responses of *Asm*$^{-/-}$ mice in three different iNKT cell-dependent disease models. First, systemic α-GalCer administration, a model of iNKT cell-mediated hepatitis, resulted in reduced serum levels of alanine transaminase (ALT) and cytokines including interleukin (IL)-4 and interferon (IFN)-γ in *Asm*$^{-/-}$ mice compared to wild-type mice (Fig. 2a). Second, we observed that delayed type hypersensitivity (DTH) induced by oxazolone, a model for skin allergy that is dependent on iNKT cell activation[17] was reduced in *Asm*$^{-/-}$ mice, as defined by weight loss after skin sensitization (Fig. 2b) and ear swelling following oxazolone re-challenge (Fig. 2c). Lastly, we examined concanavalin A (ConA) hepatitis, a model of hepatic injury driven by direct (CD1d-independent) activation of iNKT cells[18]. In this model, tissue damage (Fig. 2d-e) and damage-associated elevations of serum transaminases (Fig. 2f) were dramatically reduced in *Asm*$^{-/-}$ mice, which was accompanied by a reduction in the expression of iNKT cell-associated cytokines such as IL-4 after 6 hours and IFN-γ after 24 hours in the serum (Fig. 2f). Such diminished *in vivo* responses to α–GalCer, oxazolone and ConA in *Asm*$^{-/-}$ mice are consistent with the decreased levels of iNKT cells and/or impaired presentation of agonistic CD1d-restricted antigens. Together, these models document the importance of ASM in regulating iNKT cell-dependent inflammation.

**ASM deficiency leads to altered lipid antigen presentation and thymic iNKT cell selection**

We hypothesized that the reduction in iNKT cells observed in *Asm*$^{-/-}$ mice was due to reduced presentation of CD1d-restricted antigens involved in positive selection of iNKT cells in the thymus. In contrast to classical MHC class I- and II-restricted T

cells, which are positively selected by cortical thymic epithelial cells, iNKT cells are selected by CD1d-expressing thymocytes[4]. We observed that, although CD1d expression was unaffected by ASM-deficiency in young mice and only slightly reduced in the thymus of adult mice (Supplementary Fig. 4), thymocytes from both adult and young (2 weeks old) *Asm*$^{-/-}$ mice compared to wildtype thymocytes led to reduced IL-2 release by co-cultured iNKT hybridomas in response to CD1d-restricted presentation of endogenous (self) and exogenous (α–GalCer) antigens (Fig. 3a). Of note, similar cell surface expression of CD1d in young *Asm*$^{-/-}$ and wildtype mice suggests that defects in CD1d-restricted antigen presentation in the absence of ASM are not an indirect consequence of altered CD1d trafficking as the latter typically affects CD1d cell surface expression[19,20]. Further, the iNKT hybridomas used are ASM-proficient, which rules out iNKT cell intrinsic defects due to the lack of ASM as the cause of reduced activation. Inhibition with 19G11, a monoclonal antibody directed against CD1d, confirmed that iNKT cell activation in these assays was CD1d-dependent (Supplementary Fig. 5a).

Given the dramatic reduction iNKT cells in *Asm*$^{-/-}$ mice and the defects of *Asm*$^{-/-}$ thymocytes in CD1d-restricted antigen presentation (Fig. 3a), we investigated whether ASM deficiency affects thymic development of iNKT cells. To this end, we characterized thymic iNKT-cell development[4]. As expected from the reduction in thymic iNKT cells in *Asm*$^{-/-}$ mice (Fig. 1c-d), ASM deficiency was associated with dramatically reduced absolute numbers of iNKT cells at stages 1, 2 and 3 of thymic development (Fig. 3b, left). Within the small population of thymic iNKT cells in *Asm*$^{-/-}$ mice, the relative proportion of cells in stage 2 was increased and stage 3 reduced

compared to wildtype mice (Fig. 3b, right). These results suggest a major bottle-neck at the earliest stages of iNKT development in the thymus when ASM is absent.

To rule out that these developmental differences were due to an intrinsic defect in iNKT cells in *Asm*$^{-/-}$ mice rather than an abnormality in antigen presentation resulting in altered iNKT cell positive selection, we generated mixed bone marrow chimeras in which irradiated *Jα18*$^{-/-}$ recipients received bone marrow from *Jα18*$^{-/-}$ mice, which are ASM sufficient and express CD1d but do not give rise to iNKT cells due to deficiency of the invariant TCR *Jα* segment[21], mixed 1:1 with bone marrow from either *Asm*$^{-/-}$ or wildtype mice. In this experiment, functional CD1d was provided by *Jα18*$^{-/-}$ thymocytes which should allow for unimpaired iNKT cell development of the precursor cells in the *Asm*$^{-/-}$ bone marrow which are the only source of iNKT cells in this experiment. In line with this hypothesis, iNKT cells derived from *Asm*$^{-/-}$ compared to wildtype bone marrow were observed at similar abundance in the thymus, spleen and liver (Fig. 3c). These studies ruled out a cell-intrinsic defect in iNKT cells in the developing thymus of *Asm*$^{-/-}$ mice. Further, reconstitution of irradiated CD45.2$^{+}$ *Asm*$^{-/-}$ mice with bone marrow from wildtype ASM-expressing CD45.1$^{+}$ mice restored iNKT cells (Fig. 3d and e). These studies demonstrate that iNKT cell defects in *Asm*$^{-/-}$ mice arise from the bone marrow-derived radiosensitive compartment. Control experiments with irradiation of *Asm*$^{-/-}$ mice followed by transfer of *Asm*$^{-/-}$ bone marrow were not associated with an increase in the abundance of iNKT cells (Supplementary Fig. 5b).

Similar to thymocytes, CD11c$^{+}$ DCs from spleens of young and adult *Asm*$^{-/-}$ mice were less able to stimulate the endogenous reactivity of the non-invariant NKT cell

hybridoma 14S.6 and the iNKT cell hybridoma 24.8[22] (Fig. 3f). Additionally, we observed decreased presentation of endogenous and exogenous (α-GalCer) lipid antigens to the 24.7 and DN32.D3 iNKT cell hybridomas in comparison to DCs from wildtype mice (Fig. 3g). The activation of iNKT cells was CD1d-restricted and abolished by antibody-mediated blockade of CD1d (Supplementary Fig. 5c). By direct staining using a monoclonal antibody recognizing the complex of α-GalCer bound to CD1d on the cell surface, it was evident that reduced iNKT cell activation resulted from reduced loading of CD1d with α-GalCer (Fig. 3h). Finally, MHC class II-restricted antigen presentation of ovalbumin by DCs, which requires lysosomal processing of the model antigen ovalbumin, to T cells from OT-II mice[23], was unperturbed in *Asm*$^{-/-}$ mice, thus excluding general defects in lysosomal antigen processing and presentation of antigens to T cells (Fig. 3i). Together, these data demonstrate that ASM-deficiency limits the ability of thymocytes and DCs to load and present CD1d-associated antigens resulting in defects in thymic development and maturation of iNKT cells.

**ASM deficiency in humans is associated with reduced abundance of iNKT cells and an altered iNKT cell phenotype**

To extend these studies to humans, we investigated whether a similar defect in CD1d-restricted antigen presentation can be detected in patients with NPD-A and -B who are deficient in ASM. To this end, we used lentiviral transduction to introduce human CD1d into Epstein-Barr virus (EBV)-transformed B cells from an NPD type B patient and three healthy controls (Supplementary Fig. 6a). While CD1d expression in NPD lymphoblasts was within the range observed for controls (Supplementary Fig. 6a), the CD1d-transfected NPD lymphoblasts exhibited decreased CD1d-restricted

presentation of α–GalCer to the iNKT hybridoma 58ab[24] compared to similarly transfected control lymphoblasts (Fig. 4a). Given reduced iNKT cell numbers in *Asm*$^{-/-}$ mice, we analyzed the abundance of iNKT cell levels in peripheral blood of NPD-A and –B patients. While iNKT cell numbers showed variation in healthy controls in line with previous observations[25], iNKT cell frequencies in NPD-A and -B patients were significantly decreased and at the lower end of those observed in controls (Fig. 4b-c and Supplementary Table 1). The median relative abundance of iNKT cells among NPD-A and -B patients was 0.014% (Interquartile range (IQR) 0.012%-0.029%) compared to 0.086% (IQR 0.037%-0.18%) among the control subjects (P=0.0004). In addition, the phenotype of the residual iNKT cells in NPD patients differed from controls as shown by a dramatically altered $CD4^+/CD8^+$ iNKT cell ratio and reduced expression of the maturation marker CD161[26], which is acquired through interactions with CD1d in the periphery[4] (Supplementary Fig. 6b). This reduction in iNKT cells in human NPD subjects is in marked contrast to observations in Gaucher's disease[27], Fabry's disease[28] and Niemann-Pick disease Type C[29], all of which represent sphingolipid-dependent lysosomal storage diseases, wherein iNKT cell levels are not affected. In contrast to iNKT cells, no alterations were detected in the abundance of conventional T cells or their $CD4^+$ and $CD8^+$ subpopulations (Fig. 4d and Supplementary Fig. 6c). In conclusion, the iNKT cell defects observed in NPD patients suggest a role of ASM in the regulation of human iNKT cell development, in line with the observations made in *Asm*$^{-/-}$ mice. The absence of defects in conventional T cells in NPD patients further suggests that such alterations are specific to iNKT cells and that they do not result from general defects in lysosomal antigen processing. This is in line with unaltered MHC class II-restricted antigen presentation

(Fig. 3i) and unaffected frequencies of conventional T cells (Supplementary Fig. 3a) in *Asm*$^{-/-}$ mice.

We also evaluated a potential correlation between ASM activity and iNKT cell abundance and function among healthy humans. To this end, we determined ASM activity in peripheral blood mononuclear cells (PBMC) and correlated it with peripheral iNKT cell frequency and the iNKT cell phenotype. While we did not observe a correlation between ASM activity in PBMCs and the abundance of iNKT cells, ASM activity was variable and positively correlated with the expression of CD161 and the relative proportion of iNKT cells expressing CD8 (Fig. 4e). These results suggest that ASM activity regulates CD1d and NKT cells in the periphery and/or the thymus in healthy human subjects under physiological conditions.

**ASM deficiency leads to early accumulation of sphingomyelin, which competes with agonistic lipids for binding to CD1d**

Our results so far demonstrated that deficiency in ASM is associated with impaired presentation of CD1d-associated antigens leading to defects in the positive selection of iNKT cells. We therefore analyzed whether changes in the lipidome contribute to the observed defects. To this end, we first examined the lipid content of thymi and livers of 2-week old wildtype and *Asm*$^{-/-}$ mice using mass spectrometry. The analysis of the thymus revealed an increase in sphingomyelin and DH-sphingomyelin levels with C24:1 and C16:0 being the most abundant species detected (Fig. 5a), while the levels of ceramides and DH-ceramides, the breakdown products of sphingomyelin and DH-sphingomyelin, were unaffected (Fig. 5b). In comparison, an analysis of total liver tissue exhibited a modest increase in sphingomyelin and decreased ceramide

abundance in *Asm*$^{-/-}$ relative to wildtype mice (Supplementary Fig. 7). We therefore investigated whether the species of sphingomyelin increased in *Asm*$^{-/-}$ thymi could interfere with CD1d-mediated antigen presentation. To exclude lipid effects on the APCs themselves, we used an APC-free assay with platebound CD1d[9] where sphingomyelin and α-GalCer directly compete for binding to CD1d. In addition, we used sphingomyelin concentrations that were within the range of the molar concentrations of sphingomyelin observed in thymocytes, calculated based on the average size of a thymocyte[30]. We observed that sphingomyelin 24:1 inhibited the ability of α-GalCer to stimulate the DN32.D3 hybridoma in response to plate bound CD1d, while sphingomyelin 16:0 species possessed a detectable albeit less pronounced inhibitory effect (Fig. 5c). The other sphingomyelin species that were increased in *Asm*$^{-/-}$ mice made up only a small fraction compared to the levels of 24:1 and 16:0 sphingomyelin. Nevertheless, we tested the effects of the next most elevated species and observed that 24:0 and 18:0 sphingomyelin elicited similar effects in blocking α–GalCer presentation (Fig. 5d). Direct activation of the DN32.D3 hybridoma with plate bound anti-CD3 was not influenced by the inhibitory sphingomyelin species indicating that sphingomyelin did not directly affect iNKT cell function (Supplementary Fig. 8a). Furthermore, we confirmed, using the plate-bound CD1d assay, that ASM does not directly facilitate the loading of lipids onto CD1d (Supplementary Fig. 8b). These studies indicate that ASM-deficiency is associated with accumulation of sphingomyelin species that compete with agonistic CD1d-binding lipids, thus limiting their ability to stimulate iNKT cells. Since iNKT cells are selected by antigens processed in the endolysosomal pathway[20,31] and presented by other thymocytes, we developed a novel technique for defining the lipid content of the lysosomes in thymocytes (see Methods). The identity of the purified lysosomes from

thymocytes was confirmed by the enrichment of lysosomal markers (Lamp1, Lamp2 and CtsD), but not markers for mitochondria (CoxIV), early endosomes (Rab5) nuclei (HisH3) or cytosol (GAPDH, tubulin) as determined by Western blot (magnetic fraction in Fig. 6a) and electron microscopy (Fig. 6b). Lipidomic analysis of the purified lysosome fractions demonstrated an increased ratio of the sphingomyelin species shown to be inhibitory for CD1d-restricted antigen presentation (Fig. 5c and d), relative to the total level of ceramide in *Asm*$^{-/-}$ compared to wildtype thymocytes of 2-week (Fig. 6c), 10-week (Fig. 6d) and 20-week old mice (Fig. 6e). It is notable that significantly elevated ratios of sphingomyelin species were already observed in the lysosomes of thymocytes of 2-week old mice, which is consistent with the iNKT cell defects observed at these early stages of development and thus long before other features of ASM deficiency arise.

**Sphingomyelin can displace agonistic lipids from CD1d**

Our results suggested that ASM deficiency lead to early accumulation of sphingomyelin, which competes as a non-agonistic lipid with agonistic lipids for binding to CD1d. This leads to interference with CD1d-restricted positive selection of iNKT cells in the thymus and with CD1d-dependent maturation of iNKT cells in the periphery. We therefore addressed whether sphingomyelin, in addition to its ability to compete with agonistic lipids for binding to CD1d (Fig. 5c-d), can also displace agonistic lipids that are already bound to CD1d. To this end, recombinant CD1d was loaded with sulfatide (SLF), a negatively charged agonistic lipid for non-invariant NKT cells[32,33], and incubated with increasing concentrations of sphingomyelin to address whether sphingomyelin can actively displace SLF. Indeed, successful replacement of SLF was confirmed in native isoelectric focusing (IEF) gel

electrophoresis by a band shift to the 0 position. Even at a 1:1 (sphingomyelin:SLF) molar ratio, sphingomyelin replaced approximately 50% of the bound sulfatide similar to that observed with the agonistic lipid α-GalCer (Fig. 7a). When we first loaded sphingomyelin or α-GalCer onto murine CD1d and then added sulfatide, we observed less replacement of α-GalCer compared to sphingomyelin (Fig. 7a). However, it is anticipated that these differences in affinity to CD1d are outweighed *in vivo* by the massive increase in molar abundance of sphingomyelin leading to an excess of lipids that bind to CD1d but do not provide activating signals to iNKT cells. Together, these data demonstrate that sphingomyelin can directly compete with, and replace, agonistic lipids from CD1d, consistent with its ability to interfere with CD1d-restricted antigen presentation.

**CD1d-sphingomyelin structure**

To examine the molecular basis of the aforementioned observations we determined the mouse CD1d-sphingomyelin (CD1d-SM) structure to a resolution of 1.95 Å (Table 1). A well-ordered electron density for the lipid was observed throughout the structure, with the exception of the choline group, which appeared to be flexible, since it did not form considerable contacts with CD1d (Fig. 7b-e, PDB structure ID: 6CYW). The C24:1 acyl chain of sphingomyelin was contained in the larger A' pocket, while the sphingosine was inserted into the F' pocket, similar to the binding of other glycosphingolipids such as sulfatide or α-GalCer[34,35]. In contrast to the binding of α-GalCer[34], sphingomyelin was observed to form fewer H-bond interactions with CD1d, of which the lack of an interaction with D153 was especially noticeable. In contrast, the phosphate group formed a novel contact with S76 and a salt-bridge with R79. The structure also explains why sphingomyelin is not an agonist

antigen for iNKT cells, since sphingomyelin lacks the typical α-anomerically linked hexose sugar that is the hallmark of strong iNKT cell antigens. The resolved structure agrees with the observation that once α-GalCer is bound to CD1d, it is not easily outcompeted by sulfatide, while sphingomyelin appears to interact less tightly with CD1d, supporting the notion that sulfatide can outcompete sphingomyelin more easily. However, the binding assay also revealed that CD1d bound lipids can be replaced against other lipids in a dose-dependent manner. This phenomenon is drastically different to that of peptide binding to conventional MHC I molecules, where it is difficult to replace a peptide once its bound[36].

**Treatment with recombinant human ASM can restore iNKT-levels**

Our results raised the question of whether restoration of ASM in *Asm*$^{-/-}$ mice could reverse sphingomyelin-dependent inhibition of CD1d-restricted antigen presentation or even augment presentation by wildtype cells. As *in vivo* administration of recombinant human ASM (rhASM)[37] has been shown to reverse the visceral lipid defect in *Asm*$^{-/-}$ mice[38] and is under development as treatment for Type B NPD, we reasoned that *in vivo* injection of rhASM may enhance CD1d-restricted antigen presentation and restoration of iNKT cell development. Importantly, it has been shown that rhASM is taken up into lysosomes[37], where CD1d localizes and lipid exchange occurs[39]. Indeed, one day after rhASM administration into *Asm*$^{-/-}$ (Fig. 8a) or wildtype mice (Fig. 8b), spleen DCs exhibited increased α-GalCer-induced iNKT cell activation compared to vehicle-treated mice. Of note, the ability of rhASM to increase iNKT cell activation by wildtype DCs suggests that ASM serves as a tunable factor in determining the CD1d-dependent antigen presentation capacity of DCs under constitutive conditions. We further investigated whether rhASM treatment from birth

could reverse the reduction in iNKT cell levels in *Asm*$^{-/-}$ mice. Following 2 weeks of rhASM treatment, ASM activity was significantly increased in the thymi and livers of *Asm*$^{-/-}$ treated mice (Fig. 8c) and thymic sphingomyelin abundance was reduced to that found in wildtype mice (Fig. 8d). Moreover, this was associated with an increase in iNKT cells (Fig. 8e and f). Together, these results demonstrate that rhASM enhances CD1d-restricted antigen presentation in wildtype and *Asm*$^{-/-}$ DCs and can partially restore the iNKT cell defect observed in *Asm*$^{-/-}$ mice.

## DISCUSSION

iNKT cells are a potent subset of T cells, whose activation requires tight control to prevent overt autoimmunity[8]. While previous work has focused on the identification of CD1d-associated lipids that activate iNKT cells (agonistic lipids), lipidomic studies have revealed that the vast majority of CD1d-associated lipids are non-agonistic self-lipids, derived from abundant cellular sphingolipids and glycerophospholipids[40]. This raises the question of whether the abundance of such non-agonistic CD1d-associated lipids is critical for control of iNKT cell development, CD1d-restricted iNKT cell activation and iNKT cell-mediated inflammation. Here, we have addressed this question through the study of ASM, an enzyme critical for control of the abundance of sphingomyelin, a major CD1d-associated lipid which does not activate iNKT cells. Our results demonstrate that ASM, through control of the abundance of sphingomyelin, regulates the balance between activating and non-activating CD1d-associated lipids and controls iNKT activation and development.

These studies highlight and focus attention on the important role played by inhibitory self-lipids in guiding CD1d-restricted responses and further indicate that, in addition

to exogenously derived inhibitory sphingolipids provided by the commensal microbiota[41], the host employs endogenous strategies to serve a similar purpose. The accumulation of sphingomyelin in *Asm*$^{-/-}$ mice was associated with diminished positive selection of iNKT cells in the thymus and altered maturation of iNKT cells in the thymus and the periphery[4]. This deficiency in iNKT cells also translated into altered responses in iNKT mediated disease models. Defects in the CD1d-iNKT axis observed in *Asm*$^{-/-}$ mice were paralleled by iNKT cell defects in NPD-A and B patients. These findings contrast patients with NPD-C, a disease sharing neurological phenotype but with a different molecular basis[42], that have a normal distribution of iNKT cells[29].

Given the critical role of iNKT cells in antimicrobial immunity against common respiratory pathogens such as *Pneumococcus* and *Pseudomonas spp*. [43,44], iNKT cell defects are anticipated to contribute to susceptibility of NPD-A and NPD-B patients to pneumonia, which represents the most common cause of death in these patients[45]. However, the relevance of our data extends far beyond individuals with NPD-A and NPD-B. As such, the correlation between ASM activity and the iNKT cell phenotype in healthy individuals, as well as the promotion of CD1d-restricted antigen presentation by rhASM in wildtype mice suggests that ASM functions as a major regulator of iNKT cell development and function under constitutive conditions in normal hosts. Our results may also contribute to the understanding of the variability of iNKT cell levels and subsets in humans[25]. These observations likely apply in a similar manner to other major cellular lipids that associate with CD1d and fail to activate iNKT cells. As such, our findings suggest that iNKT cell development and immunity is tightly linked to, and controlled by, cellular lipid metabolism. This has

broad implications for common immuno-metabolic diseases, such as non-alcoholic steatohepatitis, in which inflammation and tissue destruction is mediated by iNKT cells, and in which changes in lipid metabolism may indeed act as primary drivers of pathogenic iNKT cell activation through alterations in the balance between iNKT cell activating and non-activating lipids. As such, conditions that regulate ASM levels in immune cells may have important effects on iNKT cell function[2].

In conclusion, our studies pinpoint sphingomyelin as a lipid species that endogenously regulates CD1d-restricted antigen presentation by thymocytes and peripheral activation of iNKT cells in response to endogenous, as well as exogenous, stimulatory antigens. Further, we demonstrate that ASM, an enzyme localized in the lysosome, plays a critical role in regulating the levels of this important inhibitory lipid. In addition, our studies further suggest that these pathways are amenable to therapeutic manipulation not only in humans with lipid storage diseases[46], but also in circumstances wherein ASM supplementation (or blockade) may aid in promoting CD1d-restricted responses that are beneficial in the treatment of infectious diseases, autoimmunity and cancer.

## ACKNOWLEDGMENTS

This work was supported by US National Institutes of Health (NIH) grants HD28607 (MERIT Award) (to E.H.S.). DK044319, DK051362, DK053056, DK088199, the Harvard Digestive Diseases Center DK034854 (to R.S.B.). The South-Eastern Norwegian Health trust, the Unger-Vetlesen Foundation, Caroline Musæus Aarvolds fund and the Norwegian PSC research center (to E.M.). The European Research Council (ERC Starting Grant agreement no. 336528), the Deutsche Forschungsgemeinschaft (DFG) (ZE 814/4-1, ZE 814/7-1), and the DFG Excellence Cluster Center for Regenerative Therapies Dresden (CRTD) (to S.Z.). The DFG (SCHU733/14-1) (to S.S. and J.F.), and the DFG Excellence Cluster Inflammation at Interfaces Schleswig-Holstein (EXC 306) (to S.S.). This work is partially funded by FEDER Funds under the Portugal 2020 partnership agreement through Norte Portugal Regional Operational Program (Norte 2020) (Norte-01-0145-FEDER-000012). J Bame, J Danielson, A. Dias, M.L. Maia, S Torquato, J Øgaard and J Anmarkrud are thanked for invaluable technical help. We would like to thank the following physicians for patient and control subject recruitment in Portugal: T. Cardoso, N. Alegrete (CHSJoão, Porto); E. Martins and E. Silva (CHPorto, Porto); L. Ribeiro and A. Pereira (CHUCoimbra, Coimbra). We would like to acknowledge the Blood bank of CHSJoão, Porto and the NIH Tetramer Core Facility for provision of CD1d-PBS57 tetramer and CD1d monomer.

## AUTHOR CONTRIBUTIONS

EM designed, performed, and analyzed experiments with RSB. EM, SZ, and RSB wrote the manuscript. XJ, KDB, CMD, AP and CT helped with experiments. MFM and CSP provided and analyzed human samples for NKT cells. SZ provided

lentiviruses expressing CD1d and contributed to the design of experiments and the interpretation of results. JF and SS performed extraction of lysosomes. JW and DMZ performed the IEF experiments and determined the CD1d-sphingomyelin structure. AK, THK and MAE provided scientific input. SLK, JD and AHM performed MS and analyzed the lipidomics data together with EM. EHS provided *Asm*$^{-/-}$ mice and rhASM, assisted in the analysis of experiments, and reviewed the manuscript. RSB supervised the studies.

## AUTHOR INFORMATION

Correspondence and requests for materials should be addressed to espen.melum@medisin.uio.no and rblumberg@bwh.harvard.edu. EHS is consultant for Sanofi/Genzyme. MFM has received a research grant from Sanofi-Genzyme. There are no other competing financial interests.

## REFERENCES


1. Brigl, M. & Brenner, M. B. CD1: Antigen Presentation and T Cell Function. *Annu Rev Immunol* **22,** 817–890 (2004).

2. Brennan, P. J., Brigl, M. & Brenner, M. B. Invariant natural killer T cells: an innate activation scheme linked to diverse effector functions. *Nat Rev Immunol* **13,** 101 117 (2013).

3. Godfrey, D. I. & Berzins, S. P. Control points in NKT-cell development. *Nat Rev Immunol* **7,** 505 518 (2007).

4. Godfrey, D. I., Stankovic, S. & Baxter, A. G. Raising the NKT cell family. *Nat Immunol* **11,** 197 206 (2010).

5. Gapin, L., Godfrey, D. I. & Rossjohn, J. Natural Killer T cell obsession with self-antigens. *Curr Opin Immunol* **25,** 168–173 (2013).

6. Merrill, A. H. Sphingolipid and Glycosphingolipid Metabolic Pathways in the Era of Sphingolipidomics. *Chem Rev* **111,** 6387–6422 (2011).

7. Yuan, W., Kang, S., Evans, J. & Cresswell, P. Natural Lipid Ligands Associated with Human CD1d Targeted to Different Subcellular Compartments. *J Immunol* **182,** 4784 4791 (2009).

8. Salio, M., Silk, J. D., Jones, Y. E. & Cerundolo, V. Biology of CD1- and MR1-Restricted T Cells. *Annu Rev Immunol* **32,** 323–366 (2014).

9. Fox, L. M. *et al.* Recognition of lyso-phospholipids by human natural killer T lymphocytes. *Plos Biol* **7,** e1000228 (2009).

10. Smith, E. & Schuchman, E. The unexpected role of acid sphingomyelinase in cell death and the pathophysiology of common diseases. *Faseb J* **22,** 3419 3431 (2008).

11. Im, J. S. *et al.* Kinetics and Cellular Site of Glycolipid Loading Control the Outcome of Natural Killer T Cell Activation. *Immunity* **30,** 888 898 (2009).

12. Perrotta, C. & Clementi, E. Biological Roles of Acid and Neutral Sphingomyelinases and Their Regulation by Nitric Oxide. *Physiology* **25,** 64–71 (2010).

13. Zeidan, Y. H. & Hannun, Y. A. The Acid Sphingomyelinase/Ceramide Pathway: Biomedical Significance and Mechanisms of Regulation. *Current molecular medicine* 454 466 (2009). doi:CMM # 51 [pii]

14. Horinouchi, K. *et al.* Acid sphingomyelinase deficient mice: a model of types A and B Niemann–Pick disease. *Nat Genet* **10,** 288 293 (1995).

15. Truman, J.-P., Gadban, M. M., Smith, K. J. & Hammad, S. M. Acid sphingomyelinase in macrophage biology. *Cell Mol Life Sci* **68,** 3293–3305 (2011).

16. Yang, O. O. *et al.* CD1d on Myeloid Dendritic Cells Stimulates Cytokine Secretion from and Cytolytic Activity of Vα24JαQ T Cells: A Feedback Mechanism for Immune Regulation. *J Immunol* **165,** 3756–3762 (2000).

17. Nieuwenhuis, E. E. *et al.* CD1d and CD1d-restricted iNKT-cells play a pivotal role in contact hypersensitivity. *Exp Dermatol* **14,** 250 258 (2005).

18. Takeda, K. *et al.* Critical contribution of liver natural killer T cells to a murine model of hepatitis. *Proc National Acad Sci* **97,** 5498–5503 (2000).

19. Cernadas, M. *et al.* Lysosomal Localization of Murine CD1d Mediated by AP-3 Is Necessary for NK T Cell Development. *J Immunol* **171,** 4149–4155 (2003).

20. Chiu, Y.-H. *et al.* Multiple defects in antigen presentation and T cell development by mice expressing cytoplasmic tail–truncated CD1d. *Nat Immunol* **3,** 55–60 (2001).

21. Cui, J. *et al.* Requirement for Vα14 NKT Cells in IL-12-Mediated Rejection of Tumors. *Science* **278,** 1623–1626 (1997).

22. Behar, S., a Podrebarac, T., Roy, C., Wang, C. & Brenner, M. Diverse TCRs recognize murine CD1. *Journal of immunology (Baltimore, Md. : 1950)* **162,** 161 167 (1999).

23. Barnden, M. J., Allison, J., Heath, W. R. & Carbone, F. R. Defective TCR expression in transgenic mice constructed using cDNA-based α- and β-chain genes under the control of heterologous regulatory elements. *Immunol Cell Biol* **76,** 34–40 (1998).

24. Thedrez, A. *et al.* CD4 engagement by CD1d potentiates activation of CD4+ invariant NKT cells. *Blood* **110,** 251–258 (2007).

25. Zeissig, S. *et al.* Primary deficiency of microsomal triglyceride transfer protein in human abetalipoproteinemia is associated with loss of CD1 function. *J Clin Invest* **120,** 2889–2899 (2010).

26. McNab, F. *et al.* The Influence of CD1d in Postselection NKT Cell Maturation and Homeostasis. *J Immunol* **175,** 3762 3768 (2005).

27. Balreira, A., Lacerda, L., Miranda, C. & Arosa, F. A. Evidence for a link between sphingolipid metabolism and expression of CD1d and MHC-class II: monocytes from Gaucher disease patients as a model. *Brit J Haematol* **129,**

667–676 (2005).

28. Pereira, C. S. *et al.* Invariant natural killer T cells are phenotypically and functionally altered in Fabry disease. *Mol Genet Metab* **108,** 241–248 (2013).

29. Speak, A. O. *et al.* Invariant natural killer T cells are not affected by lysosomal storage in patients with Niemann-Pick disease type C. *Eur J Immunol* **42,** 1886–1892 (2012).

30. Salinas, F., Smith, L. & Goodman, J. Cell size distribution in the thymus as a function of age. *J Cell Physiol* **80,** 339 345 (1972).

31. Chiu, Y.-H. *et al.* Distinct Subsets of CD1d-restricted T Cells Recognize Self-antigens Loaded in Different Cellular Compartments. *J Exp Medicine* **189,** 103–110 (1999).

32. Jahng, A. *et al.* Prevention of Autoimmunity by Targeting a Distinct, Noninvariant CD1d-reactive T Cell Population Reactive to Sulfatide. *J Exp Medicine* **199,** 947–957 (2004).

33. Girardi, E. *et al.* Type II natural killer T cells use features of both innate-like and conventional T cells to recognize sulfatide self antigens. *Nat Immunol* **13,** 851 (2012).

34. Zajonc, D. M. *et al.* Structure and function of a potent agonist for the semi-invariant natural killer T cell receptor. *Nat Immunol* **6,** 810 818 (2005).

35. Zajonc, D. M. *et al.* Structural basis for CD1d presentation of a sulfatide derived from myelin and its implications for autoimmunity. *J Exp Medicine* **202,** 1517–1526 (2005).

36. Sette, A. *et al.* Peptide binding to the most frequent HLA-A class I alleles measured by quantitative molecular binding assays. *Mol Immunol* **31,** 813–822 (1994).

37. He, X. *et al.* Characterization of human acid sphingomyelinase purified from the media of overexpressing Chinese hamster ovary cells. *Biochimica Et Biophysica Acta Bba - Protein Struct Mol Enzym* **1432,** 251 264 (1999).

38. Miranda, S. *et al.* Infusion of recombinant human acid sphingomyelinase into niemann-pick disease mice leads to visceral, but not neurological, correction of the pathophysiology. *Faseb J* **14,** 1988 1995 (2000).

39. Bendelac, A., Savage, P. B. & Teyton, L. The Biology of NKT Cells. *Annu Rev Immunol* **25,** 297–336 (2007).

40. Cox, D. *et al.* Determination of Cellular Lipids Bound to Human CD1d Molecules. *Plos One* **4,** e5325 (2009).

41. An, D. *et al.* Sphingolipids from a Symbiotic Microbe Regulate

Homeostasis of Host Intestinal Natural Killer T Cells. *Cell* **156,** 123–133 (2014).

42. Group:, T. *et al.* Recommendations on the diagnosis and management of Niemann-Pick disease type C. *Mol Genet Metab* **98,** 152–165 (2009).

43. Nieuwenhuis, E. *et al.* CD1d-dependent macrophage-mediated clearance of Pseudomonas aeruginosa from lung. *Nat Med* **8,** 588 (2002).

44. Kinjo, Y. *et al.* Invariant natural killer T cells recognize glycolipids from pathogenic Gram-positive bacteria. *Nat Immunol* **12,** 966 974 (2011).

45. McGovern, M. M. *et al.* Morbidity and mortality in type B Niemann–Pick disease. *Genet Med* **15,** 618 (2013).

46. Platt, F. M. Sphingolipid lysosomal storage disorders. *Nature* **510,** 68–75 (2014).

## FIGURE LEGENDS

**Figure 1.** Acid sphingomyelinase deficient mice have a reduced number of iNKT cells. (a) ASM activity was measured in tissues from WT mice (n=4) using a colorimetric assay in tissue lysates generated by repeated freeze/thaw cycles from the indicated tissues. The results are representative of two independent experiments. (b) Representative flow cytometry of lymphocytes from spleens in WT and *Asm*$^{-/-}$ mice visualizing the number of iNKT cells as defined by a PBS57-loaded CD1d tetramer and CD3. (c) Percentages of iNKT cells among lymphocytes in thymus, spleen and liver of age and gender matched WT (n=5) and *Asm*$^{-/-}$ (n=4) mice defined by PBS57-loaded CD1d tetramer and CD3 positivity. The results are representative of three independent experiments. (d) Absolute numbers of iNKT cells in thymus, spleen and liver of age and gender matched WT (n=5) and *Asm*$^{-/-}$ (n=5) mice defined by PBS57-loaded CD1d tetramer and TCRβ. The results are representative of three independent experiments. (e) Representative flow cytometry of lymphocytes from spleens in WT and *Asm*$^{-/-}$ mice at 2 weeks of age, visualizing the number of iNKT cells as defined by a PBS57-loaded CD1d tetramer and CD3. In all panels the mean values are shown with the error bars representing the SEM. *P*-values were calculated by a two-sided t-test. *$P<0.001$, **$P<0.0001$

**Figure 2.** NKT mediated disease models are affected by ASM deficiency. (a) Age and gender matched WT and *Asm*$^{-/-}$ mice were injected with 2 μg α-galactosylceramide i.p. Cytokine levels were determined in serum 4 and 24h after injection and ALT levels in serum 24h after the injections. Results are representative of three independent experiments. (b) Oxazolone was used to sensitize WT and *Asm*$^{-/-}$ mice on

the skin at day 0. The mice were followed daily with weight measurements and the values reflect the weight relative to the starting weight. Results are representative of three independent experiments. (c) Five days after the skin sensitization the mice received a re-challenge by application of oxazolone to the ear. Ear swelling was measured by a sensitive micrometer and the lines indicate the increase in ear thickness. (d) Quantification of necrotic areas in WT and *Asm*$^{-/-}$ mice injected with concanavalin A. The results represent pooled results from three independent experiments. (e) Representative H&E stained tissue sections from WT and *Asm*$^{-/-}$ mice 24h after injection with concanavalin A. The black bar indicates 200µm. Results are representative of three independent experiments. (f) Age and gender matched WT and *Asm*$^{-/-}$ mice were injected with concanavalin A. Cytokine and ALT levels were determined in serum 6 and 24h after injection. The results represent pooled results from three independent experiments. In all panels the mean values are shown with the error bars representing the SEM. *P*-values were calculated by two-sided t-test (panel a), 2-way ANOVA (panel b and c) or the two-sided Mann-Whitney test (panel d and f). **P*<0.05, ***P*<0.01, ****P*<0.001

**Figure 3.** Lipid antigen presentation by thymocytes and DCs from ASM deficient mice is reduced and bone-marrow transfer restores iNKT cell levels in *Asm*$^{-/-}$ mice. (a) Thymocytes were incubated with α-galactosylceramide for 4h or left untreated, followed by addition of the indicated NKT hybridomas. Thymocytes from both young (2-week old) and adult *Asm*$^{-/-}$ mice were used as indicated. (b) The graphs show absolute (left) and relative (right) numbers of iNKT cells in different thymic developmental stages in *Asm*$^{-/-}$ mice and WT mice. Stage 1 was defined as CD24$^{lo}$CD44$^{lo}$NK1.1$^{lo}$, stage 2 as CD24$^{lo}$CD44$^{hi}$NK1.1$^{lo}$ and stage 3 as

$CD24^{lo}CD44^{hi}NK1.1^{hi}$. The results are representative of two independent experiments. (c,d,e) Bone-marrow chimeras were made by mixing $J\alpha18^{-/-}$ and WT (n=5) or $Asm^{-/-}$ (n=8) bone-marrow transferred to irradiated $J\alpha18^{-/-}$ recipients (c) or by transfer of WT $CD45.1^{+}$ bone-marrow to $Asm^{-/-}$ mice (n=7) that was compared to non-irradiated $Asm^{-/-}$ mice not receiving bone-marrow (n=6) (d,e). The graphs demonstrate the percentage of CD1d-PBS57 tetramer positive cells among TCRβ positive cells (iNKT cells) three months after bone-marrow transfer. In panel c the results are representative of two independent experiments while in panel e the results represent pooled results from three independent experiments. The dot plots in panel d show representative plots from the livers of a non-irradiated $Asm^{-/-}$ mouse not receiving bone-marrow and an $Asm^{-/-}$ mouse receiving WT bone-marrow. (f,g) $CD11c^{+}$ DCs were extracted from spleens with magnetic beads and co-cultured with the indicated NKT hybridomas. Prior to co-culture 24.7 α-GC loaded and DN32.D3 α-GC loaded were loaded with α-galactosylceramide for 4h. DCs from both young (2 weeks) and adult $Asm^{-/-}$ mice were used as indicated. (h) $CD11c^{+}$ DCs were extracted from spleens and incubated α-galactosylceramide for 4 or 24 hours and stained with an antibody recognizing α-galactosylceramide bound to CD1d in three technical replicates. The results are representative of two independent experiments. (i) DCs from WT and $Asm^{-/-}$ mice were loaded with ovalbumin and cultured with ovalbumin reactive T cells from OT-II mice. In all co-culture experiments (panels a, f, g and i) IL-2 levels were measured in three independent wells 20-24 hours after addition of the indicated NKT hybridomas, and all these results are representative of three independent experiments. In all panels the mean values are shown with the error bars representing the SEM. *P*-values were calculated by two-sided t-test in all panels

except in panel h where 2-way ANOVA was used. *$P$<0.05, **$P$<0.01, ***$P$<0.001, ***$P$<0.0001, NS not significant

**Figure 4.** Human ASM deficiency is associated with reduced CD1d-restricted antigen presentation to iNKT cells and a reduced level of iNKT cells. (a) EBV transformed B-cells were transduced with a lentiviral construct coding for human CD1d, loaded with α-galactosylceramide and cultured with the 58ab hybridoma. The graph shows the mean IL-2 levels from three independent wells with cells from the indicated individuals. The results are representative of three independent experiments. (b) Representative dot plots from a NPD patient and a healthy control. The percentages indicate the percentage of iNKT cells among lymphocytes. (c,d) The graphs demonstrate the level of iNKT (c) and T cells (d) in patients with NPD (n=5) compared to healthy controls (n=70). The percentages indicate the percentage of iNKT cells or T cells among lymphocytes. (e) ASM activity in PBMCs was measured using a colorimetric assay and the iNKT cell phenotype was examined by flow-cytometry in healthy controls (n=25). The graphs show the correlation between ASM activity and the percentage of CD8 positive/CD161 positive cells among iNKT cells. In panel a the mean values are shown with the error bars representing the SEM. In panel c the line indicates the median value. *P*-values were calculated with 1-way ANOVA with Bonferroni's method for multiple correction (panel a), the two-sided Mann-Whitney test (panel c and d), two-sided Pearson's correlation (panel e) *$P$<0.05, **$P$<0.01 ***$P$<0.001, NS not significant

**Figure 5.** Lipids increased in *Asm*$^{-/-}$ mice block antigen presentation. (a) Sphingomyelin levels in the thymus of 2-week old *Asm*$^{-/-}$ (n=2) and WT (n=2) mice were quantified by mass spectrometry. The graphs show the mean levels of sphingomyelins and DH-sphingomyelins with carbon chains of different lengths. (b) Ceramide levels in the thymus of 2-week old *Asm*$^{-/-}$ (n=2) and WT (n=2) mice were quantified by mass spectrometry. The graphs show the mean levels of ceramides, DH-ceramides, hexosylceramides and DH-hexosylceramides. (c, d) Plate-bound CD1d was incubated with α-galactosylceramide and a dose range of the indicated sphingomyelin species before addition of the iNKT hybridoma DN32.D3. The graphs demonstrate the mean level of IL-2 in three independent wells in the culture supernatants 16-24 hours after addition of iNKT cells. The stars indicate the significance levels compared with cytokine secretion when no sphingomyelin was added (0 nM). The results are representative of three independent experiments. In all panels the mean values are shown with the error bars representing the SEM. *P*-values were calculated with 1-way ANOVA with Bonferroni's method for multiple correction. **P*<0.001, ***P*<0.0001

**Figure 6.** Lipids blocking CD1d-restricted antigen presentation are increased in thymic lysosomes of two week old *Asm*$^{-/-}$ mice. (a) Lysosomes were extracted from thymi of WT and *Asm*$^{-/-}$ mice using magnetic beads. The figure shows the lysosome identity for the samples by western blot with markers for different cellular compartments of the whole tissue lysate, the magnetic bead purified lysosomes, the soluble non-bound material, mitochondria enriched sediment and the non magnetic microsomal debris. The results are representative of three independent experiments.

The blot images were cropped so all markers could be visualized together. (b) Electron microscopy images of the purified lysosome fraction. The red arrows indicate lysosomes. The black bar represents 100 nm. The results are representative of three independent experiments. (c) Sphingomyelin levels in the magnetic bead fraction were quantified by mass spectrometry. The graphs show the ratios of the indicated sphingomyelin species to the total level of ceramide in 2-week old WT and *Asm*$^{-/-}$ mice. (d,e) Ratios of the indicated sphingomyelin species to the total level of ceramide in 10 (panel d) and 18-20 (panel e) week old WT and *Asm*$^{-/-}$ mice. In all panels the mean values are shown with the error bars representing the SEM. *P*-values were calculated by two-sided t-test (c, d and e). **P*<0.05, ***P*<0.01 ****P*<0.001 Lysosomal-associated membrane protein 1 (Lamp1), lysosome marker; Lysosomal-associated membrane protein 2 (Lamp2), lysosome marker; Cytochrome c oxidase subunit 4 isoform 1 (Cox IV), mitochondria marker; Cathepsin D (CtsD), 35 kDa (mature) lysosomal marker, 55 kDa (immature) cytosol marker; Histone H3 (HisH3), nuclei marker; Ras-related protein Rab-5 (Rab5), early endosome marker; Glyceraldehyde 3-phosphate dehydrogenase (GAPDH), cytosol marker.

**Figure 7.** Mouse CD1d-sphingomyelin crystal structure. (a) Comparison using a lipid competition assay of the ability of sphingomyelin (top panel) and α-galactosylceramide (middle panel) to outcompete sulfatide pre-loaded onto mCD1d, in a dose dependent manner, from equimolar ratio (1:1) to 9-fold molar excess of lipid compared to mCD1d-SLF complexes. Sulfatide has a single negative charge and migrates on the IEF gel to position -1, while replacement with the uncharged lipids

sphingomyelin and α-galactosylceramide results in a gel shift to position 0. Pre-loaded sphingomyelin can be outcompeted by sulfatide, but α-galactosylceramide forms a more stable interaction with CD1d and cannot be outcompeted in this *in vitro* assay (bottom panel). The results are representative of two independent experiments. (b) Mouse CD1d-sphingomyelin crystal structure overview of the CD1d (grey)-$\beta_2$M (light blue) complex presenting sphingomyelin (yellow) between the α1 and α2 helices. (c) 2FoFc electron density drawn as a blue mesh around the lipid and contoured at 1σ. (d) H-bond interactions (blue dashed lines) of CD1d residues with sphingomyelin. (e) H-bond interactions (blue dashed lines) of CD1d residues with α-galactosylceramide.

**Figure 8.** Pharmacological ASM treatment in *Asm*$^{-/-}$ mice restores iNKT cells. (a-b) CD11c$^+$ DCs were extracted from spleens of *Asm*$^{-/-}$ mice (a) or WT mice (b) treated with one dose of rhASM (5μg/g) 12-16 hour prior to extraction and loaded with α-galactosylceramide for 4h. The indicated iNKT hybridomas were added and IL-2 levels were measured in three independent wells after 20-24 hours. The results are representative of three independent experiments. (c) WT and *Asm* $^{-/-}$ mice were treated every other day from birth with rhASM (5μg/g). The graphs demonstrate the ASM activity levels in the liver and thymus of vehicle treated and rhASM treated *Asm*$^{-/-}$ and WT mice 2 days after the last enzyme injection. (d) The graphs demonstrate the levels of the blocking sphingomyelin species as measured by mass spectrometry after treatment with rhASM. (e) Representative dot-plot from the liver of a vehicle treated and a rhASM treated *Asm*$^{-/-}$ mouse. The cells are gated on the lymphocyte population and TCRβ positive cells. The percentages indicate the CD1d-

PBS57 tetramer positive cells. (f) iNKT cell levels at the age of 2 weeks in the thymus, spleen and liver of mice that were treated with rhASM or vehicle as indicated in the graphs. In panels c, d and f the numbers represent the pooled results from 3 independent experiments with vehicle treated ($Asm^{-/-}$ (n=8) and WT (n=5)) and rhASM treated ($Asm^{-/-}$ (n=6) and WT (n=10)) mice. The hypothesis tested using the t-test was that rhASM would increase iNKT cell abundance in $Asm^{-/-}$ mice. In all panels the mean values are shown with the error bars representing the SEM. *P*-values were calculated by two-sided t-test. *$P<0.05$, **$P<0.01$ ***$P<0.001$

| | mCD1d-sphingomyelin C24:1$^{+}$ |
|---|---|
| **Data collection** | |
| Space group | $P2_12_12_1$ |
| Cell dimensions | |
| *a*, *b*, *c* (Å) | 42.1, 105.3, 106.4 |
| α, β, γ (°) | 90 |
| Resolution (Å) | 50-1.95 (2.00-1.95)* |
| $R_{sym}$ | 11.9 (58.4) |
| $I / \sigma I$ | 23.4 (2.5) |
| Completeness (%) | 97.8 (82.5) |
| Redundancy | 4.2 (3.9) |
| | |
| **Refinement** | |
| Resolution (Å) | 50-1.95 |
| No. reflections | 33,561 |
| $R_{work}$ / $R_{free}$ | 22.3 / 25.6 |
| No. atoms | 3,420 |
| Protein | 2,990 |
| Ligand/ion | 112 |
| Water | 318 |
| *B*-factors | |
| Protein | 33.4 |
| Ligand/ion | 51.1 |
| Water | 38.9 |
| R.m.s. deviations | |
| Bond lengths (Å) | 0.008 |
| Bond angles (°) | 1.11 |

+ One crystal was used for data collection. *Values in parentheses are for highest-resolution shell.

**Table 1.** Data collection and refinement statistics for the CD1d-sphingomyelin structure.

1

## ONLINE METHODS

### Mouse models

*Asm*$^{-/-}$ mice have been described earlier as a mouse model for Niemann-Pick disease[14]. These mice are on a C57BL/6 background and had been backcrossed for >10 generations. The mouse line was maintained by breeding heterozygote mice (*Asm*$^{+/-}$ x *Asm*$^{+/-}$) since *Asm*$^{-/-}$ mice develop a neurological disease at an advanced age. The litters were genotyped by PCR (conditions available upon request). Mice used in the experiments were age and gender matched. Adult mice were defined as > 6 weeks of age. wildtype littermates generated through the *Asm*$^{+/-}$ x *Asm*$^{+/-}$ breeding were used as controls. To generate bone-marrow chimeras wildtype bone marrow from C57BL/6 mice carrying CD45.1 that we were able to trace using flow-cytometry were utilized. In the experiments with mixed bone marrow chimeras, bone marrow from *Jα18*$^{-/-}$ mice was mixed at a 1:1 ratio with bone marrow from *Asm*$^{-/-}$ or wildtype mice. The CD45.1 (strain 2014) and *Jα18*$^{-/-}$ mice (strain 30524) models are commercially available through Jackson Laboratories (Bar Harbour, Maine, USA). OT-II mice (strain 4194) used to acquire ovalbumin reactive T cells are also commercially available through Jackson Laboratories. The number of mice included in each individual experiment was based on prior experience in the laboratory with similar experiments. No animals were excluded from the reported experiments. Animals were allocated to each experimental group based on genotype and age/gender without randomization and no blinding was performed. All mice were housed in a specific pathogen free facility with food and water *ad libitum* in accordance with the set forth by the Harvard Medical Area Standing Committee on Animals and the Norwegian Food Safety Authority (Mattilsynet).

**Bone marrow chimeras**

Recipient mice were irradiated two times with 600 rad one day prior to injection of bone marrow. Bone marrow was extracted from donor mice from the femur by flushing with PBS, washing the cells and adjusting the concentration. For the mixed bone marrow chimeras, bone-marrow from *Jα18*$^{-/-}$ and *Asm*$^{-/-}$ or wildtype was mixed 1:1. One million cells were injected through the tail vein. The mice were then kept on acidic water for 4 weeks and observed for general well being. After 3 months the engraftment and iNKT cell percentages were evaluated by flow cytometry. Engraftment was judged by CD45.1$^{+}$ percentage among lymphocytes.

**α–GalCer hepatitis**

Age and gender matched mice were injected 2 μg α–GalCer i.p. Four hours after injection the mice were bled from tail vein, and 24 hours after the injection the mice were sacrificed and blood collected by cardiac puncture. IL-4 and IFN-γ were measured in the serum by ELISA (BD Biosciences, Franklin Lakes, New Jersey, USA). ALT was measured by a colorimetric assay (Stanbio, Boerne, Texas, USA).

**Concanavalin A hepatitis**

ConA (Sigma-Aldrich, St. Louis, Missouri, USA) was dissolved in PBS and injected through the tail vein at a dose of 13.5 mg/kg. Only male mice were used in these experiments. The mice were monitored hourly for well-being and blood sampled after 6h. At 24h the mice were sacrificed and liver and blood were sampled. IL-4 and IFN-γ were measured in the serum by ELISA (BD Biosciences). ALT was measured by a colorimetric assay (Stanbio). Liver sections were stained with hematoxylin and eosin (H&E) and the sections were scored by a semiautomatic algorithm for necrotic areas.

**Oxazolone skin painting and induced delayed type hypersensitivity**

At day 0 the abdominal skin of the mice was shaved. Then 150 µl 3% oxazolone dissolved in 3:1 ethanol:acetone was applied to the skin to sensitize the mice. The mice were followed daily with weight measurements. Five days after the skin sensitization the mice received a re-challenge by application of 20 µl 1% oxazolone dissolved in 1:1 acetone:sunflower oil to the ear. A sensitive micrometer was used to measure ear swelling the following days.

**Genotyping**

Mouse tails or mouse ear biopsies were digested in lysis buffer (100 mM Tris-HCl, pH 8.5, 5 mM EDTA, 0.2% SDS, 200 mM NaCl and proteinase K (Roche, Basel, Switzerland)) overnight at 55 C. Genomic DNA was phenol-extracted and isopropanol precipitated.

**Niemann Pick disease patients and healthy controls**

Five patients were analyzed using flow-cytometry of PBMCs, one NPD-A (1 year old) and four NPD-B patients (three adults and a 10 year old patient). In addition, 70 control subjects were studied using flow-cytometry of PBMCs, 15 children and 55 adults (blood donors). The children's control group consisted of children undergoing orthopedic surgery, without infections, underlying chronic illness or taking medication. For correlation of iNKT phenotype and ASM activity blood samples from adult healthy controls were obtained from blood donors (from buffy coats) from the Blood Bank of Centro Hospitalar de São João, Porto, Portugal. The study was approved by the Ethical Committees of the participating hospitals. The participants or

their legal representatives gave written consent to participate in the study. Blood samples were collected and processed within 24h after blood withdrew. PBMCs were isolated by density centrifugation before staining with fluorochrome conjugated antibodies or tetramers. The recruitment of NPD patients for generating lymphoblasts was approved by the institutional review board at the Icahn School of Medicine. Further details on the recruitment can be found in the Life Sciences Reporting Summary.

**Cell culture**

The murine NKT hybridomas 24.7, 24.8, 14.S6 and DN32.D3 were maintained in DMEM supplemented by 10% Fetal bovine serum (FBS), 100 units/mL of penicillin, 100 µg/mL of streptomycin, and 0.25 µg/mL of amphotericin B (Antibiotic-Antimycotic, Gibco®, Grand Island, New York, USA). Regular and transduced human EBV-transformed cells and the 58ab hybridoma were maintained in RPMI supplemented by 10% FBS, 100 units/mL of penicillin, 100 µg/mL of streptomycin, and 0.25 µg/mL of amphotericin B. Lentiviral transduction of EBV-transformed cells with a construct carrying human *CD1D* was performed as earlier described[25].

**Immunomagnetic isolation of lysosomes**

The isolation of lysosomes from murine tissue was performed according to Fritsch *et al.* [47]. In brief, tissue was thawed in 500 µl homogenization buffer (HB: 15 mM HEPES, pH7.4, 250 mM sucrose, 0.5 mM $MgCl_2$ containing complete protease inhibitor and Cyanase nuclease (SERVA Electrophoresis GmbH, Heidelberg, Germany)) followed by 3 rounds of careful sonication (10 sec, amp 2.5 at 4 °C using a cooled cup resonator (G. Heinemann, Schwäbisch Gmünd, Germany) in a total

volume of 1 ml, followed by centrifugation for 4 min at 1500 x g. The resulting supernatant was loaded on a 16% Iodixanol/HB cushion and centrifuged for 1 h at 150k x g. The resulting floating fraction was aspirated carefully from the cushion and diluted to 750 µl with HB. 2 µg of anti-Lamp1 antibody (Santa Cruz Biotechnology, Dallas, USA, catalog number sc-8098) was added and incubated for 30 min rolling at 4°C. 5 µl protein G microbeads (Miltenyi Biotec, Bergisch Gladbach, Germany, catalog number #130-071-101) were added followed by another 30 min incubation. Samples were then loaded to a HOKImag magnetic isolation device (Hoock GmbH, Kiel, Germany) for organelle pulldown. The eluate was finally sedimented by centrifugation for 1 h at 20000 xg and used for downstream application.

**Lipidomics**

The sphingolipids were quantified by extracting them from the cells (after spiking with an internal standard cocktail from Avanti Polar Lipids, Alabaster, AL, Catalog #LM-6005) with analysis by liquid chromatography, electrospray-ionization tandem mass spectrometry using an API 4000 QTrap (SCIEX, Framingham, MA, USA) as previously described[48].

**SDS-PAGE and Western blot**

For SDS-PAGE, sedimented organelles were resuspended in 15 µl modified RIPA buffer (50mM TRIS-HCl [pH 7.5], 150mM NaCl, 1% NP-40, 1% Triton X-100, 1mM EDTA, 0.25% Na-deoxycholate) and protein concentration was determined by BCA (Pierce, Waltham, MA, USA). For SDS-PAGE anyKD gels (Bio-Rad, Hercules, CA, USA) were used and 3 µg of protein were loaded. Proteins were transferred to PVDF membrane (Carl-Roth, Karlsruhe, Germany). The membranes were blocked with 5%

skimmed milk in TBST and incubated over night with the primary antibody diluted 1:500-1:5,000 in 5% skimmed milk. The peroxidase conjugated secondary antibodies were incubated for 1 h diluted 1:10,000 in 5% skimmed milk. Blots were developed using the ECL kit and films from GE Healthcare (Chicago, IL, USA). The following antibodies were used: anti-Lamp1 (Southern Biotech, Birmingham, AL, USA, catalog number 9835-01), anti-Lamp2 (Southern Biotech, catalog number 9840-01), anti-CoxIV (Santa Cruz Biotechnology, catalog number sc-292052) anti-HisH3 (Cell Signaling, Danvers, MA, USA, catalog number #4499S), anti-Rab5 (Santa Cruz Biotechnology, catalog number sc-598), anti-Cathepsin D (Millipore, Burlington, MA, USA, catalog number Ab2, IM16), anti-GAPDH (Proteintech, Rosemont, IL, USA, catalog number HRP-60004), anti-Tubulin (Proteintech, catalog number HRP-66031).

**Electron microscopy**

EM was performed as described previously[47]. After sedimentation, isolated lysosomes were fixed in 3% glutaraldehyde/PBS, followed by overnight washing in 0.1 M phosphate buffer. Samples were dehydrated and then embedded in araldite. Ultrathin sections were treated with uranyl acetate and lead citrate. Images were acquired on a JEM1400plus (Jeol, Peabody, MA).

**Flow cytometry**

Lymphocyte populations from various murine organs were prepared as previously described[49]. In brief, the spleen and thymus were macerated to get a single cell population and passed through a filter and the liver retrogradely perfused through the portal vein and macerated followed by density centrifugation. The lymphocytes were

suspended in 2% FBS in PBS. To avoid unspecific staining the Fc-receptors were blocked by using an anti-mouse CD16/32 antibody (clone 93, BioLegend, San Diego, USA, catalog number 101302) and stained with the appropriate fluorochrome conjugated monoclonal antibodies and a CD1d tetramer loaded with PBS57 (from the National Institute of Health tetramer core facility). The following antibodies were used for staining murine samples: anti-mouse CD3e (clone 145-2C11, BD Biosciences, catalog number 553066), anti-mouse TCRβ (clone H57-597, BD Biosciences, catalog number 553170), anti-mouse TCRβ (clone H57-597, BioLegend, catalog number 109212), anti-mouse CD45.1 (clone A20, BioLegend, catalog number 110728), anti-mouse CD45.2 (clone 104, BD Biosciences, catalog number 553772), anti-mouse CD1d (clone 1B1, BD Biosciences, catalog number 553846), anti-mouse CD11c (clone HL3, BD Biosciences, catalog number 553801), anti-mouse TCRβ (clone H57-597, BioLegend, catalog number 109212), anti-mouse CD44 (clone 1M7, BioLegend, catalog number 103031), anti-mouse CD24 (clone M1/69, BioLegend, catalog number 101821), anti-mouse NK1.1 (clone PK136, BioLegend, catalog number 108724), anti-mouse CD3 (clone 145-2C11, BD Biosciences, catalog number 553066), anti-mouse CD4 (clone RM4-5, BioLegend, catalog number 100528), anti-mouse CD8 (clone 53-6.7, BioLegend, catalog number 100714), anti-mouse TCR g-d (clone UC7-13DS, BioLegend, catalog number 107504), anti-mouse CD304 (clone 3E12, BioLegend, catalog number 145207), anti-mouse CD1d-aGalCer (clone L363, eBioscience, San Diego, CA, USA, catalog number 12-2019-82) and the murine CD1d tetramer loaded with PBS57 (from the National Institute of Health tetramer core facility). For evaluating CD1d expression on transduced EBV-lines anti-human CD1d (clone 51.1, BioLegend, catalog number 350308) was used. Flow data were

acquired using a MACSQuant Analyser (Miltenyi Biotec) and a BD FACSVerse™ (BD Biosciences).

For staining of the samples from Niemann-Pick disease patients and healthy controls the staining mixture was composed of anti-human CD3 (clone UCHT1, eBioscience, catalog number 17-0038-42), anti-human CD3 (clone SK7, eBioscience, catalog number 45-0036-42), anti-human CD4 (clone RPA-T4, eBioscience, catalog number 25-0049-42), anti-human CD8 (clone RPA-T8, eBioscience, catalog number 47-0088-42) and anti-human CD161 (clone HP-3G10, eBioscience, catalog number 53-1619-42) antibodies and the human CD1d tetramer loaded with PBS57 (from the National Institute of Health tetramer core facility). Patient and control samples were acquired on a 3-laser BD FACS Canto™ II flow cytometer using BD FACSDiva™ software (BD Biosciences). Estimation of absolute cell counts was done using CountBright™ Absolute Counting Beads (Molecular Probes, Eugene, OR). The analyses were performed using the FlowJo software (Tree Star, Ashland, OR).

**Cell-based antigen-presentation assays**

DCs were extracted from the spleens of mice using CD11c selection beads (Miltenyi Biotec). Thymocytes were prepared by passing the thymus through a 40uM strainer followed by washing in PBS. 50k DCs or 100k thymocytes were seeded in 96 flat-bottom cell-culture plates as indicated in the individual experiments. The cells were either loaded with 100 ng/ml α–GalCer or left untreated. Unloaded antigen was washed away before addition of 50-100k of the indicated NKT hybridomas. In some experiments the CD1d monoclonal antibody 19G11 (BioXCell, West Lebanon, NH, catalog number BE0000) or a corresponding isotype control (clone LTF-2, BioXCell, catalog number BE0090) were added to the cultures. In similar assays DCs were

loaded with ovalbumin and cultured with 100k CD4 T cells from OT-II mice. Cytokine secretion was measured in the culture supernatants by ELISA (BD Biosciences).

**Surface loading of antigens**

DCs were extracted from spleens as described above followed by incubation with 100 ng/ml α–GalCer. After incubation for 4 to 24 hours the cells were washed and stained with an anti-mouse α-GalCer:CD1d complex, clone L363 (eBioscience)[50]. Flow data was acquired as described under the section on flow-cytometry.

**Histological assessment of necrosis**

H&E stained liver sections were scanned using a Histech Panoramic Midi Slide Scanner (3DHISTECH, Budapest, Hungary). The resulting images were downscaled by a factor of 4. To get reliable segmentation of necrotic versus non-necrotic tissue, Ilastik 1.3.2[51], a toolkit for performing machine learning based image processing, was used. An average of 3 annotations were made for each segmentation class (background, necrotic- and normal tissue) on each of 5 cropped images that represented the overall variation of morphological phenotype among the samples. We employed all features of σ=10, and all colour- and texture-based features of σ=5. After training the random forest classifier, the entire sections of all samples were analyzed, and percentage of necrotic areas in each sample was determined.

**Enzyme replacement therapy**

Human recombinant ASM was produced as earlier described[37], briefly, human ASM was overexpressed in Chinese hamster ovary cells and purified from cell culture

media. As iNKT cell development mainly takes place at an early age we started treatment as early as possible[52]. Neonatal mice from day two of life were injected 5μg/g rhASM i.p. every other day until 2 weeks old. The mice were then sacrificed and the percentage of iNKT cells were determined by flow cytometry as described above. Samples from liver and thymus were also harvested at the same time for determination of ASM activity.

**Antigen presenting cell free antigen-presentation assays**

Monomeric mouse CD1d (NIH Tetramer Core Facility) was coated onto 96-well cell culture plates overnight (0.25 μg/well). Unbound CD1d was thoroughly washed away followed by incubation with 100 ng/ml of α–GalCer and a dose range of different sphingomyelin species for 16-24h. Unbound lipids were washed off and the α–GalCer reactive NKT hybridoma DN32.D3 was added. In the experiments evaluating a direct loading effect from rhASM a gradient of the same rhASM described above for the replacement experiments was added along with a gradient of bovine serum albumin as a negative control and Saposin-B (Cusabio, Houston, TX, USA) as a positive control[11]. These experiments were performed under neutral and acidic conditions. Cytokine secretion was measured in the culture supernatants by ELISA (BD Biosciences).

**Lipid competition assays**

Recombinant mouse CD1d was expressed and purified as previously reported[53]. CD1d was loaded with 3-times molar excess of sulfatides (bovine brain, Avanti Polar Lipids dissolved at 5 mg/ml in DMSO) in 100 mM Tris pH 7.0, 100 mM NaCl at 37˚C for 2 hours. After lipid loading, excess lipid was removed by ultrafiltration using

Amicon filter cartridges (30 kDa molecular weight cut-off). CD1d-sulfatide complexes were then incubated overnight at room temperature with increasing concentration of either sphingomyelin (C24:1) or α-GalCer. Lipids were dissolved in DMSO (5 mg/ml) and incubated with CD1d in the presence of 0.01 % tyloxapol. As a control, CD1d-sulfatide complexes were incubated with tyloxapol only. In a reversed experiment, CD1d was first loaded with 6-times molar excess of either sphingomyelin (10 mg/ml in DMSO) or α-GalCer (0.2 mg/ml in vehicle) o/n at room temperature, purified from excess lipid by ultrafiltration and incubated with 3-times molar excess of sulfatide for 1h at 30˚C, which is the minimum dose and time necessary for full loading to insect cell expressed mCD1d (not shown). 4 µl (2-4 µg) of the various CD1d-lipid loading experiments were analyzed using native IEF gel electrophoreses using pH 5-8 gels on a PhastSystem (GE Healthcare) and stained with coomassie.

**CD1d-sphingomyelin crystallization and structure determination**

CD1d was loaded with sphingomyelin as reported above. Excess lipid was removed by size exclusion chromatography using a Superdex S200 GL10/300 (GE Healthcare). CD1d-SM complexes were concentrated to 5 mg/ml and crystals were grown by sitting drop vapor diffusion while mixing 0.5 µl protein with 0.5 µl precipitate (20 % polyethylene glycol 3350, 200 mM sodium malonate pH 7.0). Crystals were flash-cooled in crystallization solution containing 20% glycerol. Diffraction data from a single crystal was collected at beamline 7.1 of the Stanford Synchrotron Lightsource. Diffraction data was processed to 1.95 Å using HKL2000 0.98[54]. Structure was determined using molecular replacement in Phaser[55], followed by iterative cycles of model building in COOT 0.8.9.2[56] and restrained refinement in REFMAC 5.8.0158[57]. Geometry restraints for sphingomyelin were obtained using the PRODRG2 server[58].

## ASM activity measurement

For ASM activity measurement tissue samples were homogenized and subjected to three freeze/thaw cycles (at least 10 minutes frozen) followed by centrifugation. The protein in the supernatant was used for subsequent assays. Protein concentrations were measured and normalized using a bicinchoninic acid assay (Pierce). The ASM activity was then measured using an ASM Activity Assay Kit (Echelon Biosciences, Salt Lake City, UT)

## Statistical analyses

All statistical analyses were carried out using Graphpad Prism 8.2 (GraphPad Software, San Diego, CA, USA). Variables were evaluated for a normal distribution either by the D'Agostino & Pearson normality test[59] or by manually examining the distribution of observations. For normally distributed variables the two-sided Student's T-test was used while for variables not fulfilling this requirement the two-sided Mann-Whitney test was used. Correlations were evaluated by Pearson's *r*. For experiments where multiple comparisons were included the 1-way ANOVA with Bonferroni's method for multiple correction was used. For time-series a 2-way ANOVA test was used. A $P$-value $< 0.05$ was considered statistically significant. Further details on study design can be found in the Life Sciences Reporting Summary.

## Data availability

The crystal structure is available at https://www.rcsb.org, PDB structure ID: 6CYW. The rest of the data that support the findings of this study are available from the corresponding authors upon request.

**REFERENCES:**


47. Fritsch, J., Tchikov, V., Hennig, L., Lucius, R. & Schütze, S. A toolbox for the immunomagnetic purification of signaling organelles. *Traffic* **20,** 246–258 (2019).

48. Shaner, R. L. *et al.* Quantitative analysis of sphingolipids for lipidomics using triple quadrupole and quadrupole linear ion trap mass spectrometers. *J Lipid Res* **50,** 1692–1707 (2009).

49. Zeissig, S., Olszak, T., Melum, E. & Blumberg, R. S. Analyzing antigen recognition by Natural Killer T cells. *Methods Mol Biology Clifton N J* **960,** 557 572 (2013).

50. Yu, K. *et al.* Production and characterization of monoclonal antibodies against complexes of the NKT cell ligand α-galactosylceramide bound to mouse CD1d. *J Immunol Methods* **323,** 11–23 (2007).

51. Sommer, C., Straehle, C., Kothe, U. & Hamprecht, F. A. ILASTIK: INTERACTIVE LEARNING AND SEGMENTATION TOOLKIT. *2011 Ieee Int Symposium Biomed Imaging Nano Macro* **1,** 230–233 (2011).

52. Olszak, T. *et al.* Microbial Exposure During Early Life Has Persistent Effects on Natural Killer T Cell Function. *Science* **336,** 489–493 (2012).

53. Wang, J. *et al.* Lipid binding orientation within CD1d affects recognition of Borrelia burgorferi antigens by NKT cells. *Proc National Acad Sci* **107,** 1535–1540 (2010).

54. Otwinowski, Z. & Minor, W. Processing of X-ray diffraction data collected in oscillation mode. *Methods Enzymol* **276,** 307–26 (1997).

55. McCoy, A. J., Grosse-Kunstleve, R. W., Storoni, L. C. & Read, R. J. Likelihood-enhanced fast translation functions. *Acta Crystallogr Sect D Biological Crystallogr* **61,** 458–464 (2005).

56. Emsley, P., Lohkamp, B., Scott, W. & Cowtan, K. Features and development of Coot. *Acta Crystallogr Sect D Biological Crystallogr* **66,** 486–501 (2010).

57. Murshudov, G. N., Vagin, A. A. & Dodson, E. J. Refinement of Macromolecular Structures by the Maximum-Likelihood Method. *Acta Crystallogr Sect D Biological Crystallogr* **53,** 240–255 (1997).

58. Schüttelkopf, A. W. & van Aalten, D. M. F. PRODRG: a tool for high-

throughput crystallography of protein–ligand complexes. *Acta Crystallogr Sect D Biological Crystallogr* **60,** 1355–1363 (2004).

59. D'Agostino, R. & Pearson, E. Tests for Departure from Normality. Empirical Results for the Distributions of b 2 and √b 1. *Biometrika* **60,** 613 (1973).

# Figure 1

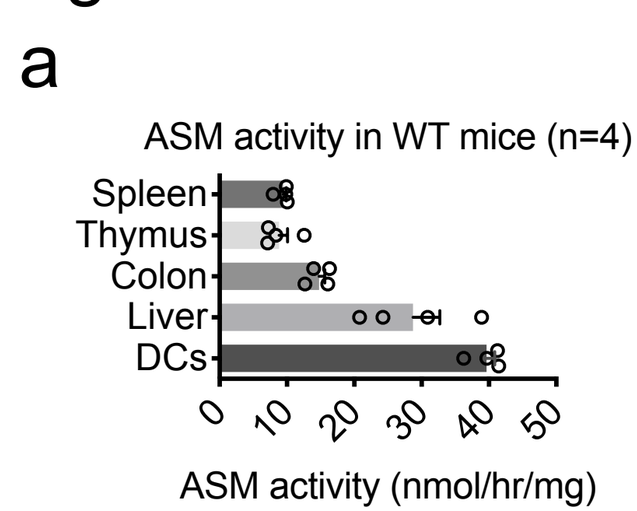
a
ASM activity in WT mice (n=4)
Spleen
Thymus
Colon
Liver
DCs
0
10
20
30
40
50
ASM activity (nmol/hr/mg)

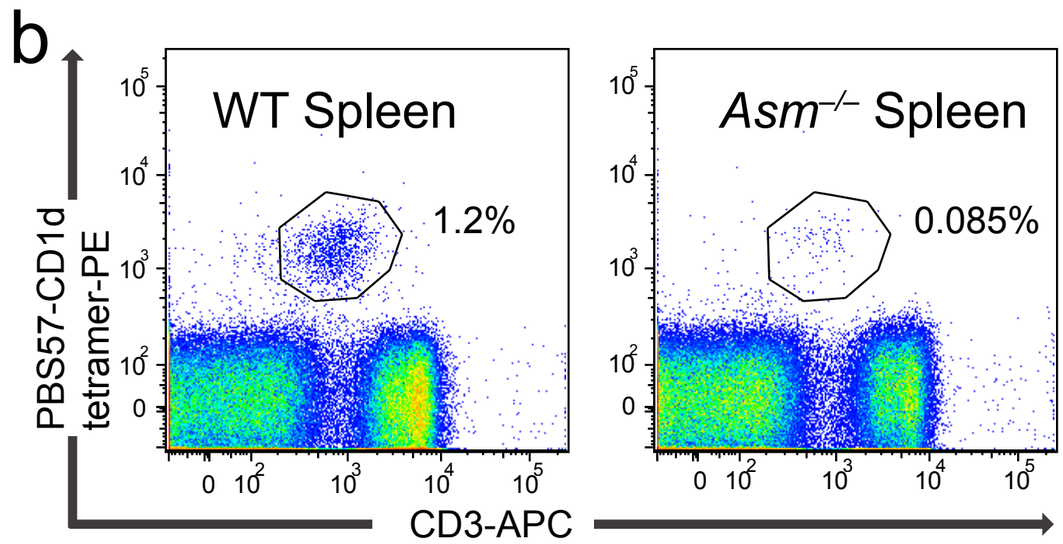
b
WT Spleen
1.2%
Asm−/− Spleen
0.085%
PBS57-CD1d tetramer-PE
CD3-APC

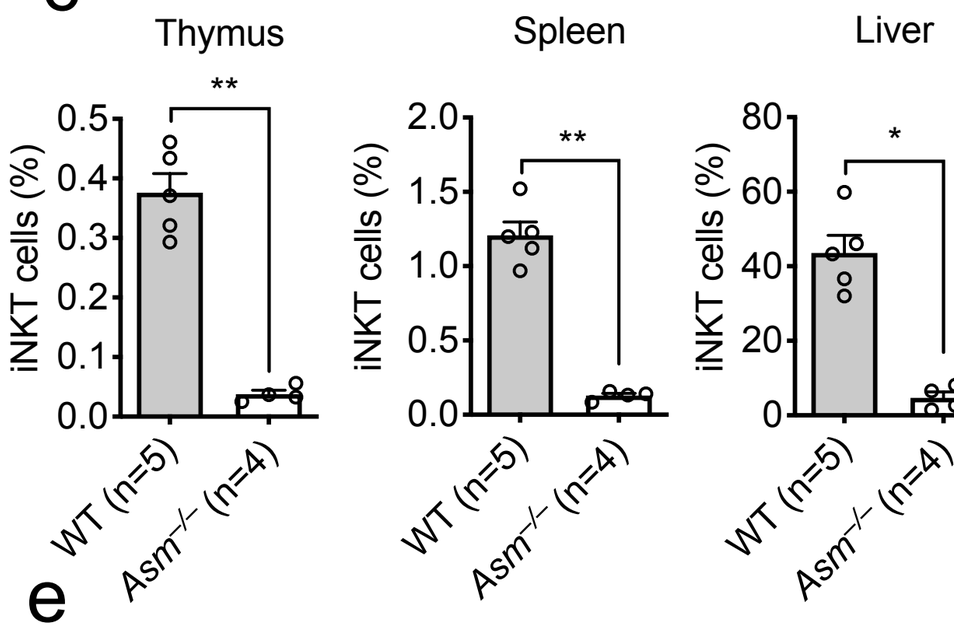
c
Thymus
Spleen
Liver
iNKT cells (%)
**
**
*
WT (n=5)
Asm−/− (n=4)

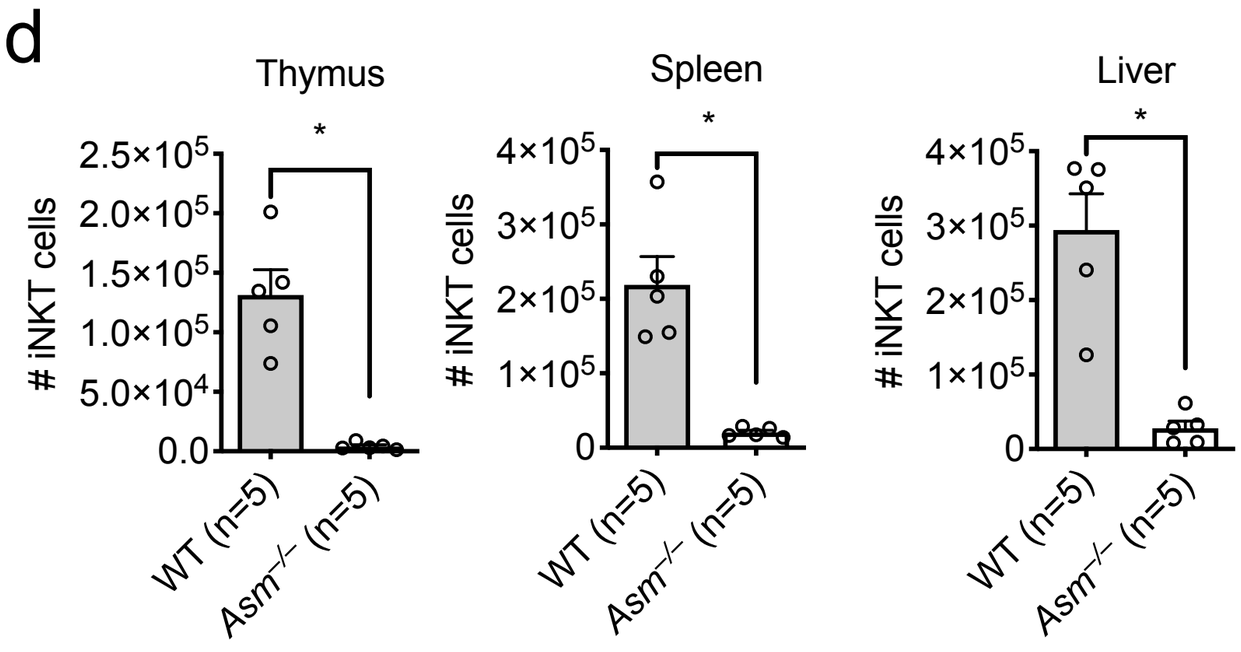
d
Thymus
Spleen
Liver
# iNKT cells
*
*
*
WT (n=5)
Asm−/− (n=5)

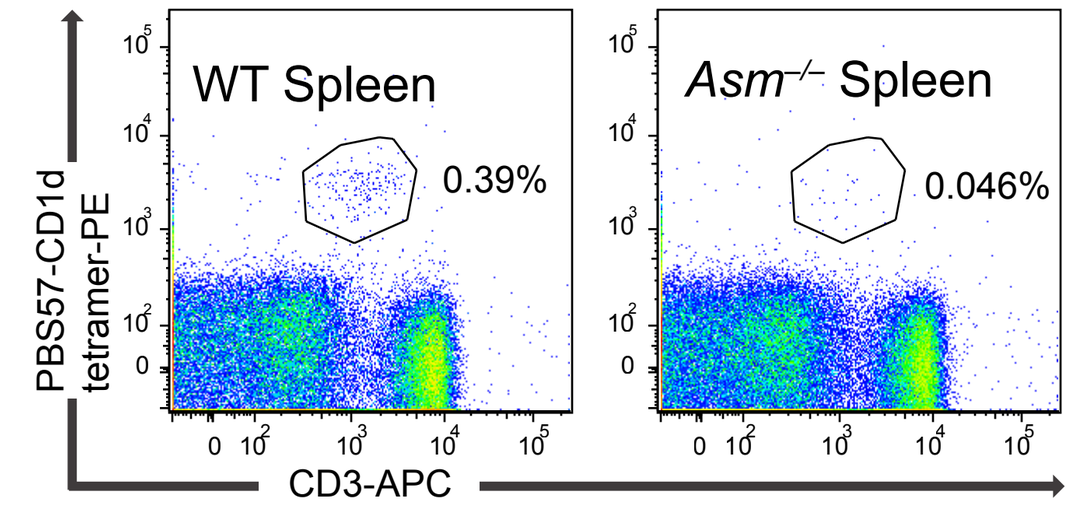
e
WT Spleen
0.39%
Asm−/− Spleen
0.046%
PBS57-CD1d tetramer-PE
CD3-APC

# Figure 2

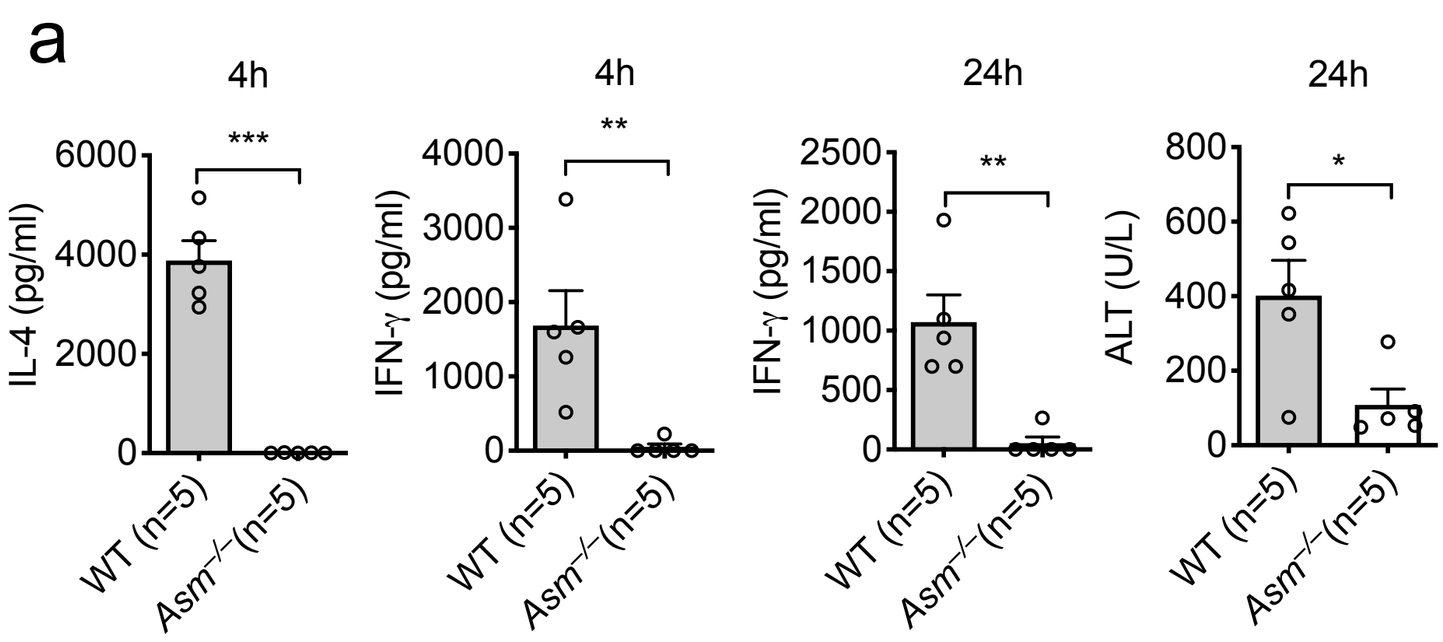
a
4h
4h
24h
24h
IL-4 (pg/ml)
IFN-γ (pg/ml)
IFN-γ (pg/ml)
ALT (U/L)
***
**
**
*
WT (n=5)
Asm−/− (n=5)

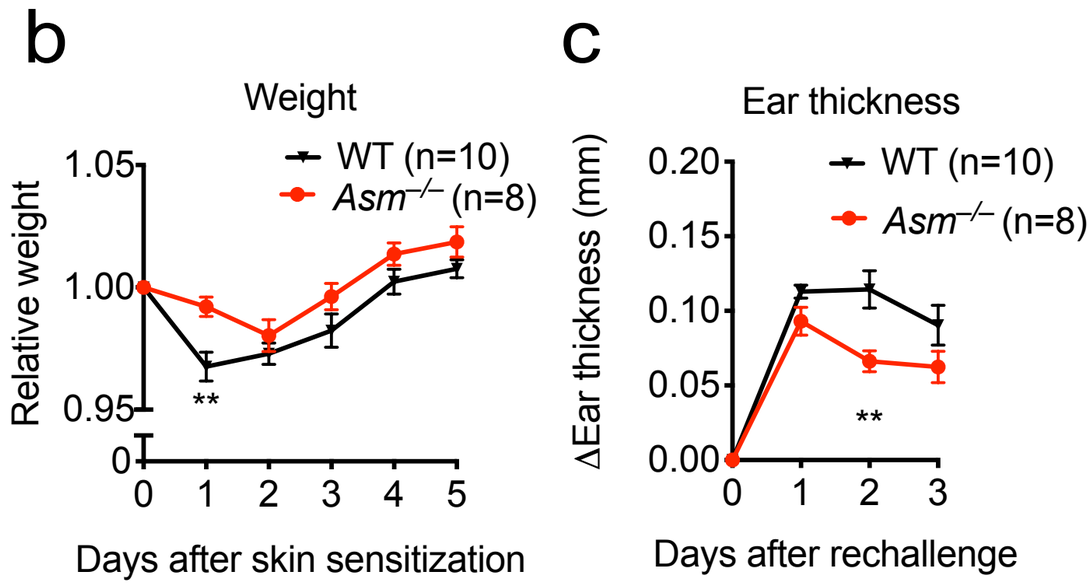
b
Weight
WT (n=10)
Asm−/− (n=8)
Relative weight
Days after skin sensitization
c
Ear thickness
WT (n=10)
Asm−/− (n=8)
ΔEar thickness (mm)
Days after rechallenge

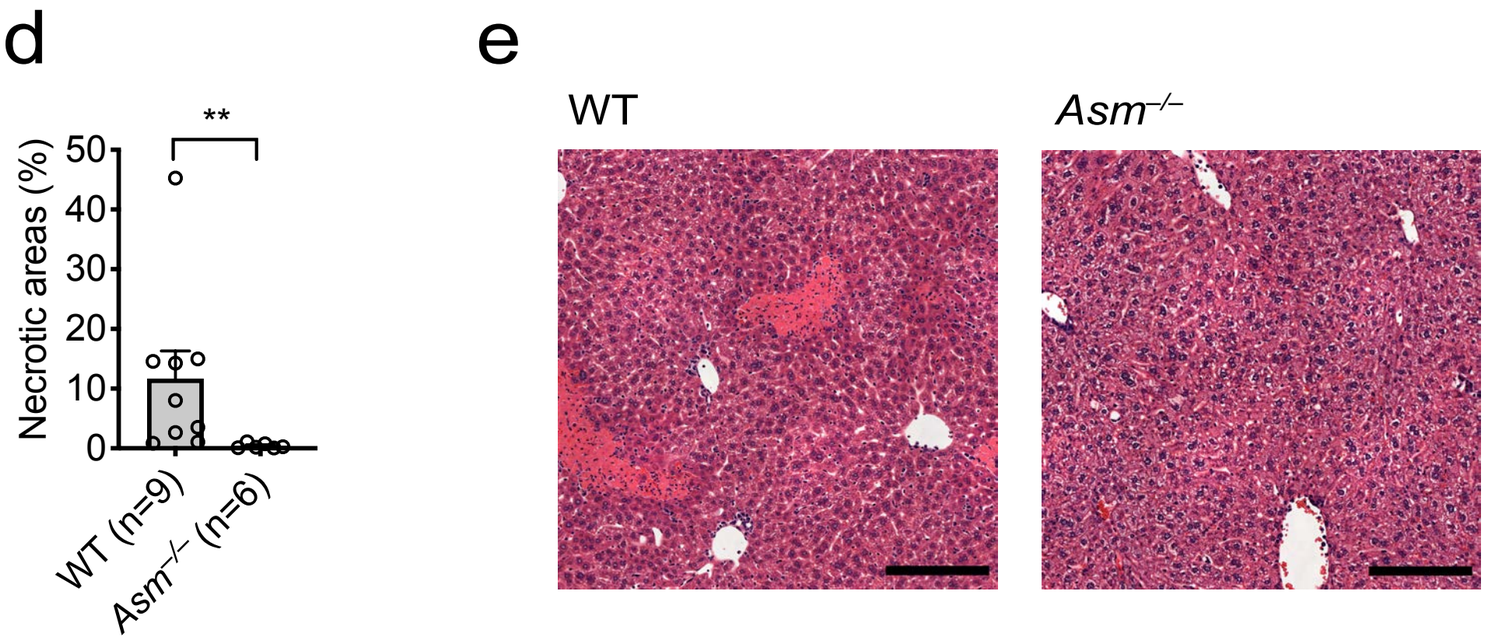
d
Necrotic areas (%)
WT (n=9)
Asm−/− (n=6)
e
WT
Asm−/−

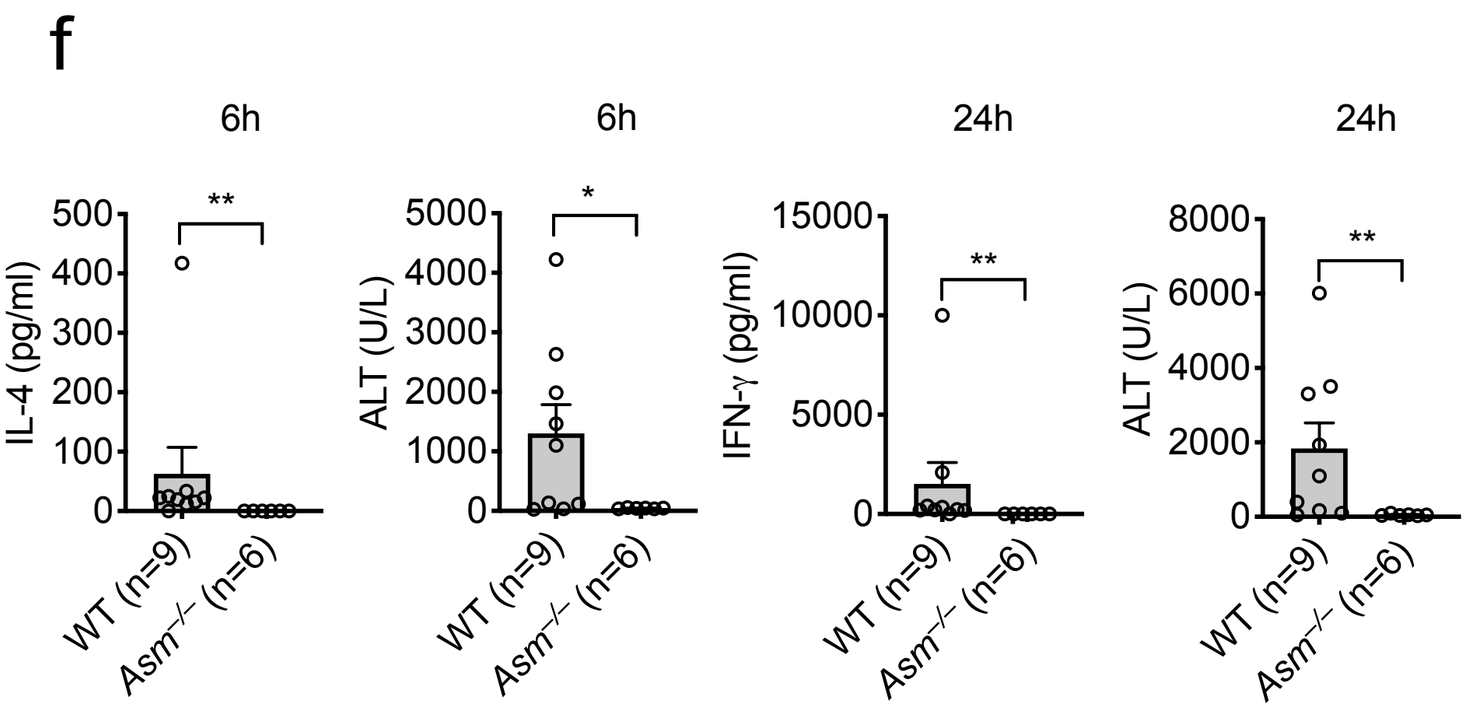
f
6h
6h
24h
24h
IL-4 (pg/ml)
ALT (U/L)
IFN-γ (pg/ml)
ALT (U/L)
WT (n=9)
Asm−/− (n=6)

Figure 3

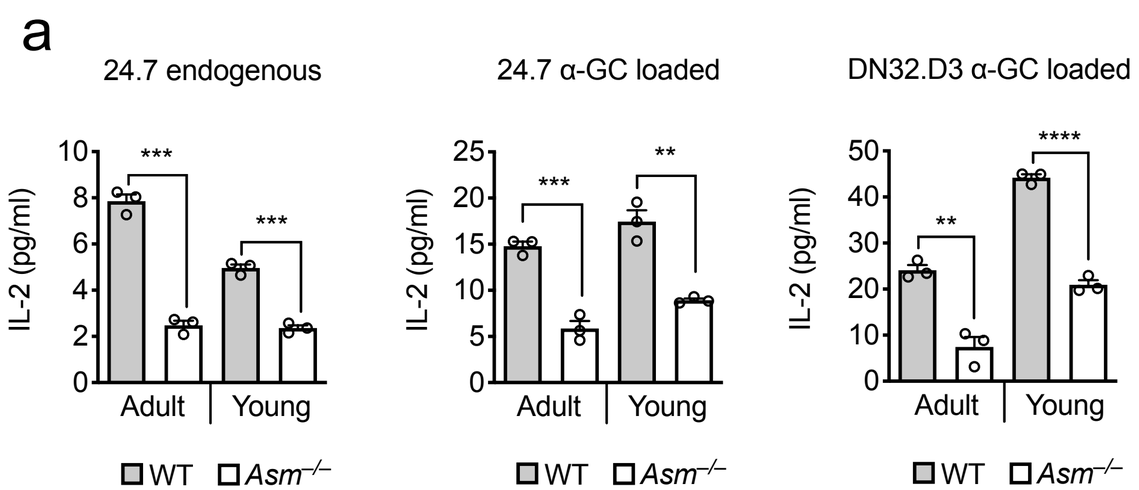
a
24.7 endogenous
24.7 α-GC loaded
DN32.D3 α-GC loaded
IL-2 (pg/ml)
Adult
Young
WT
Asm−/−

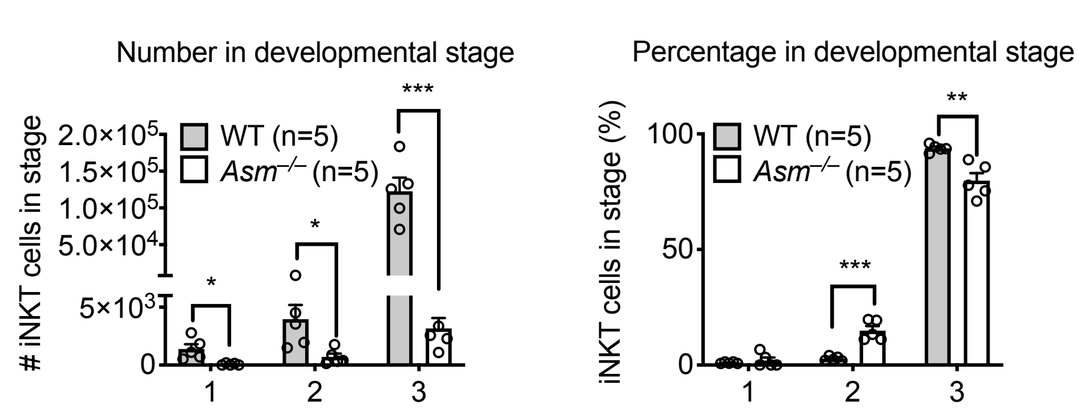
b
Number in developmental stage
Percentage in developmental stage
# iNKT cells in stage
iNKT cells in stage (%)
WT (n=5)
Asm−/− (n=5)

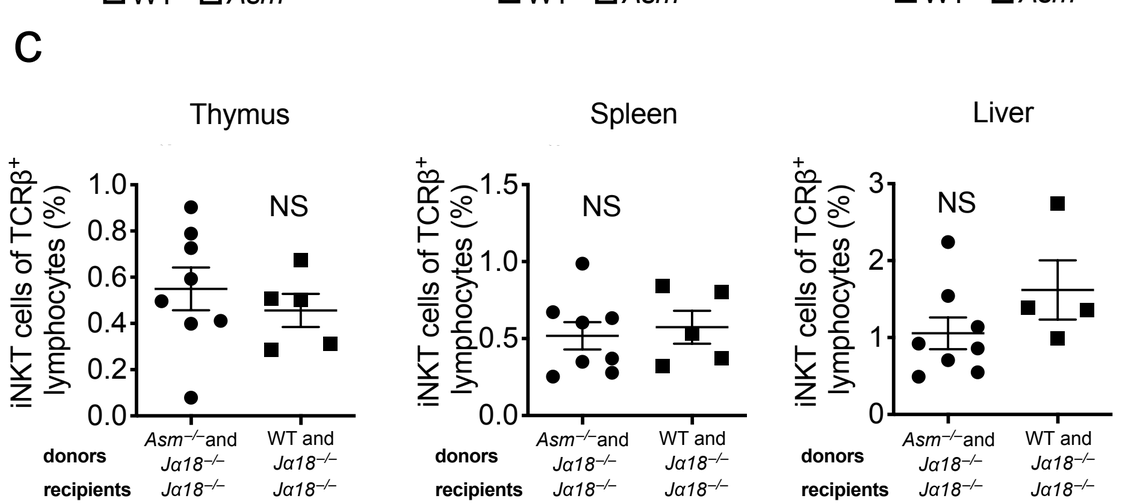
c
Thymus
Spleen
Liver
iNKT cells of TCRβ+ lymphocytes (%)
NS
donors
recipients
Asm−/− and Jα18−/−
WT and Jα18−/−

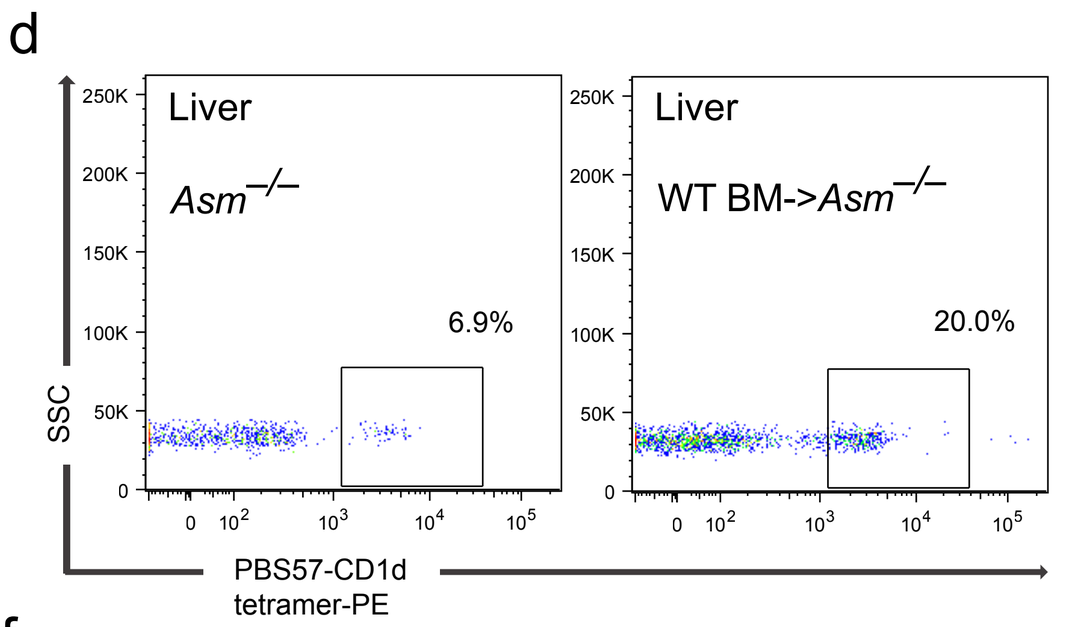
d
Liver
Asm−/−
6.9%
WT BM->Asm−/−
20.0%
SSC
PBS57-CD1d
tetramer-PE

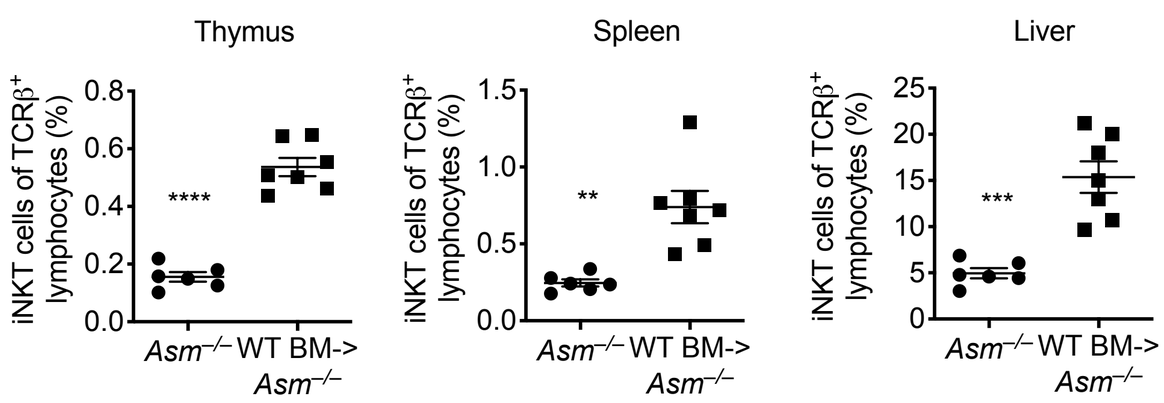
e
Thymus
Spleen
Liver
iNKT cells of TCRβ+ lymphocytes (%)
Asm−/−
WT BM-> Asm−/−

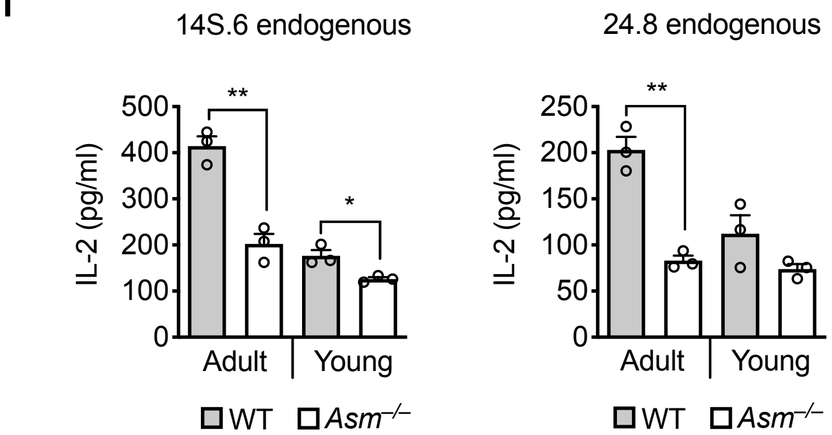
f
14S.6 endogenous
24.8 endogenous
IL-2 (pg/ml)
Adult
Young
WT
Asm−/−

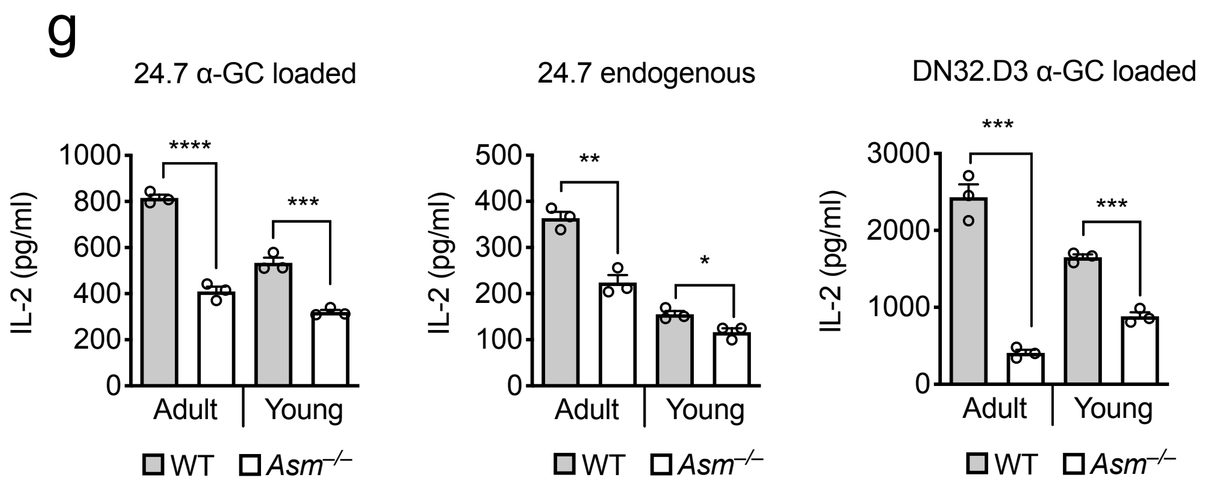
g
24.7 α-GC loaded
24.7 endogenous
DN32.D3 α-GC loaded
IL-2 (pg/ml)
Adult
Young
WT
Asm−/−

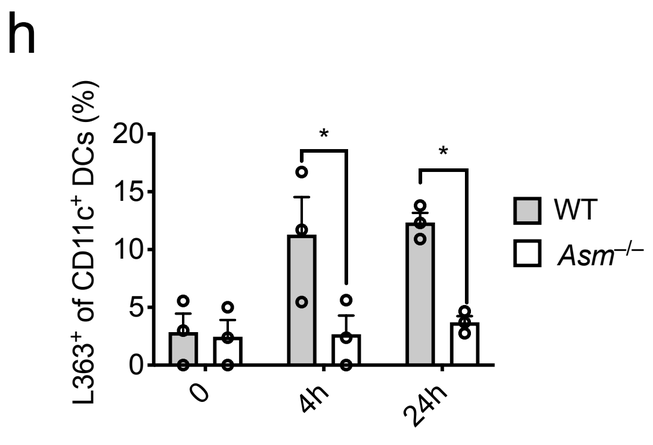
h
L363+ of CD11c+ DCs (%)
0
4h
24h
WT
Asm−/−

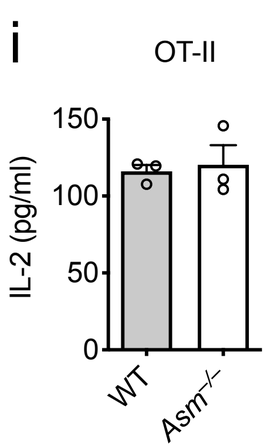
i
OT-II
IL-2 (pg/ml)
WT
Asm−/−

# Figure 4

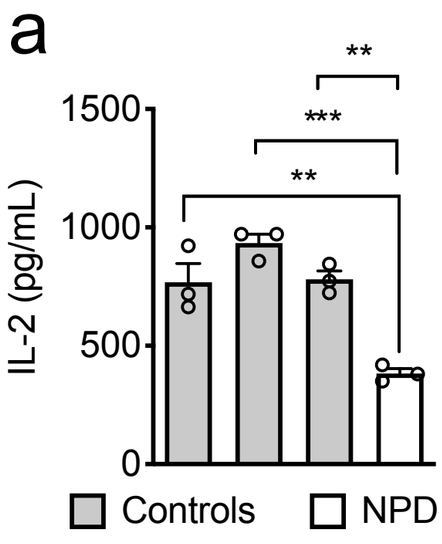
a
IL-2 (pg/mL)
1500
1000
500
0
**
***
**
Controls
NPD

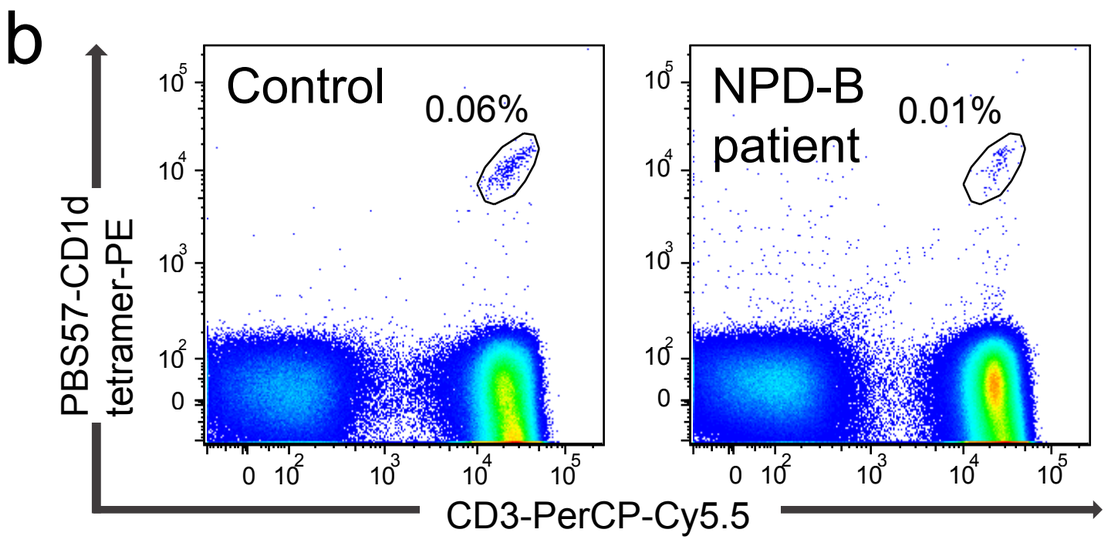
b
Control
0.06%
NPD-B
patient
0.01%
PBS57-CD1d
tetramer-PE
CD3-PerCP-Cy5.5

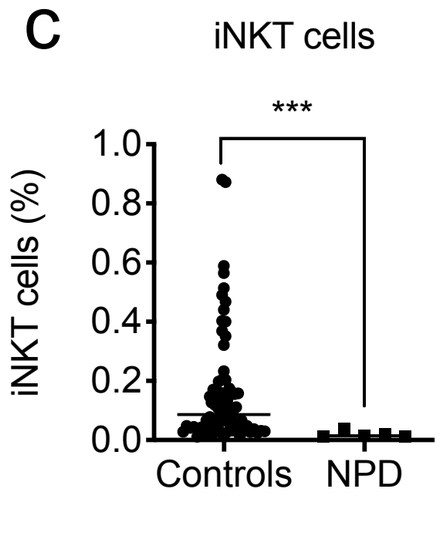
c
iNKT cells
***
iNKT cells (%)
1.0
0.8
0.6
0.4
0.2
0.0
Controls
NPD

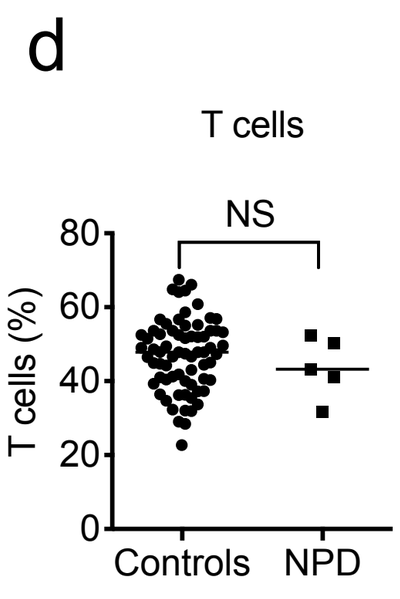
d
T cells
NS
T cells (%)
80
60
40
20
0
Controls
NPD

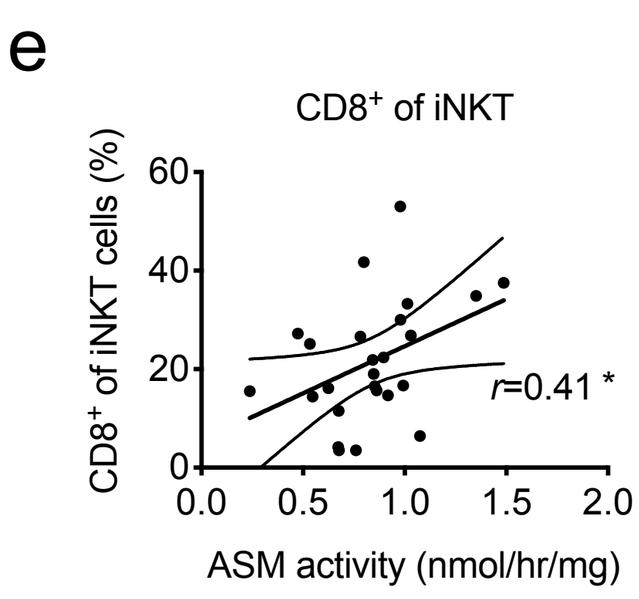
e
CD8+ of iNKT
CD8+ of iNKT cells (%)
60
40
20
0
r=0.41 *
0.0
0.5
1.0
1.5
2.0
ASM activity (nmol/hr/mg)

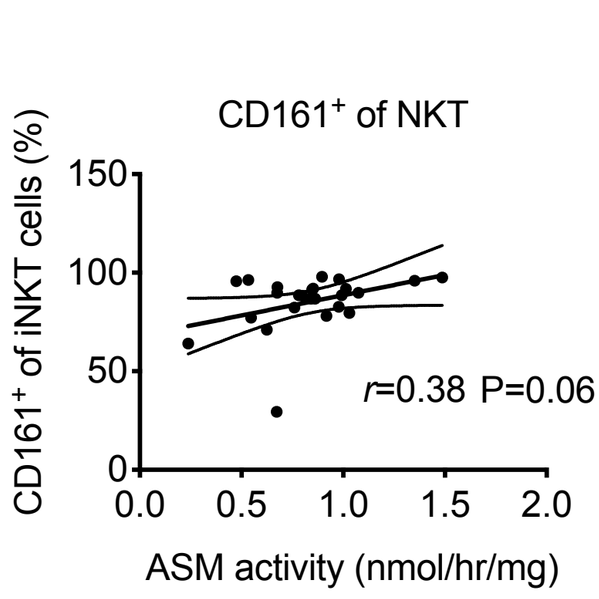
CD161+ of NKT
CD161+ of iNKT cells (%)
150
100
50
0
r=0.38 P=0.06
0.0
0.5
1.0
1.5
2.0
ASM activity (nmol/hr/mg)

# Figure 5


a
Sphingomyelins
WT
Asm−/−
C26
C26:1
C24
C24:1
C22
C20
C18
C16
0
20
40
60
80
pmol/million cells
b
Ceramides
0
2
4
6
8
10
pmol/million cells
Hexosylceramides
0
5
10
15
20
pmol/million cells
DH-Sphingomyelins
0
2
4
6
8
pmol/million cells
DH-Ceramides
0.00
0.01
0.02
0.03
pmol/million cells
DH-Hexosylceramides
0.00
0.05
0.10
0.15
pmol/million cells
c
Sphingomyelin C24:1
Sphingomyelin C16:0
IL-2 (pg/mL)
8000
6000
4000
2000
0
0
25
50
100
250
500
1000
Concentration (nM)
d
Sphingomyelin C18:0
Sphingomyelin C24:0

# Figure 6

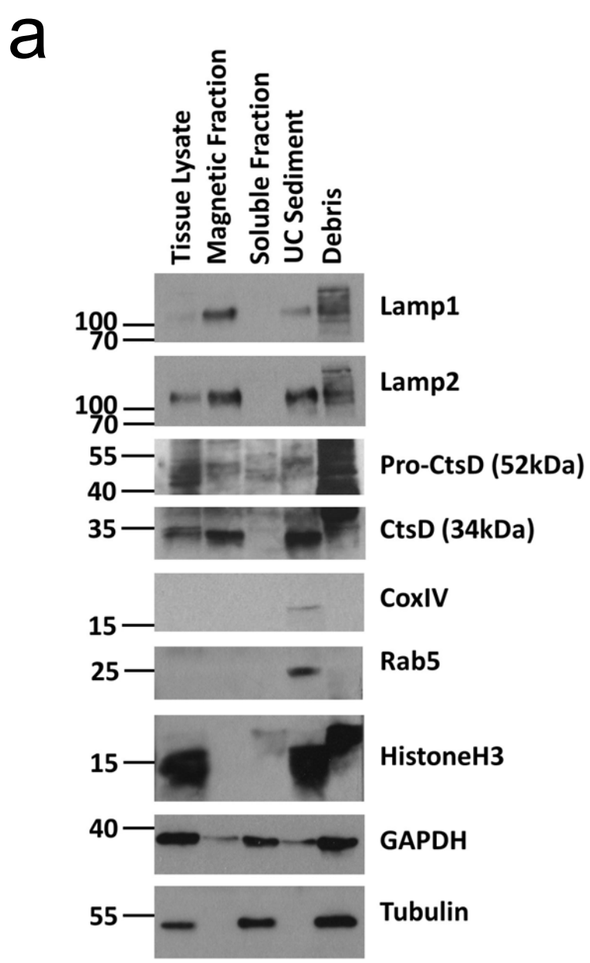
a
Tissue Lysate
Magnetic Fraction
Soluble Fraction
UC Sediment
Debris
100
70
Lamp1
100
70
Lamp2
55
40
Pro-CtsD (52kDa)
35
CtsD (34kDa)
CoxIV
15
25
Rab5
15
HistoneH3
40
GAPDH
55
Tubulin

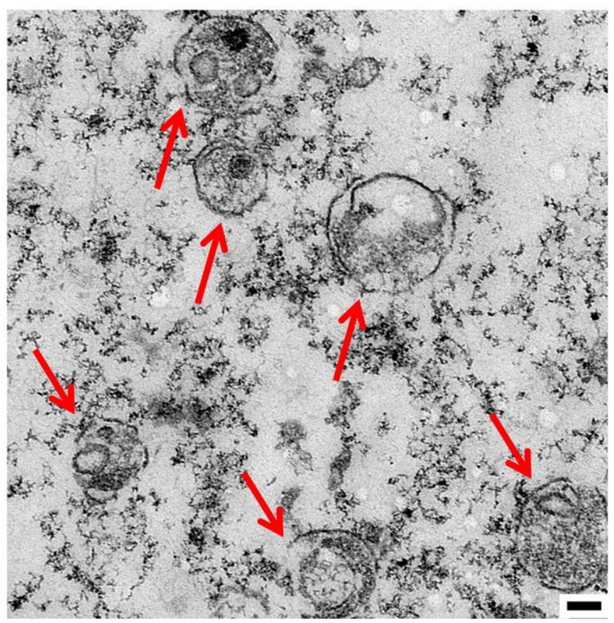
b

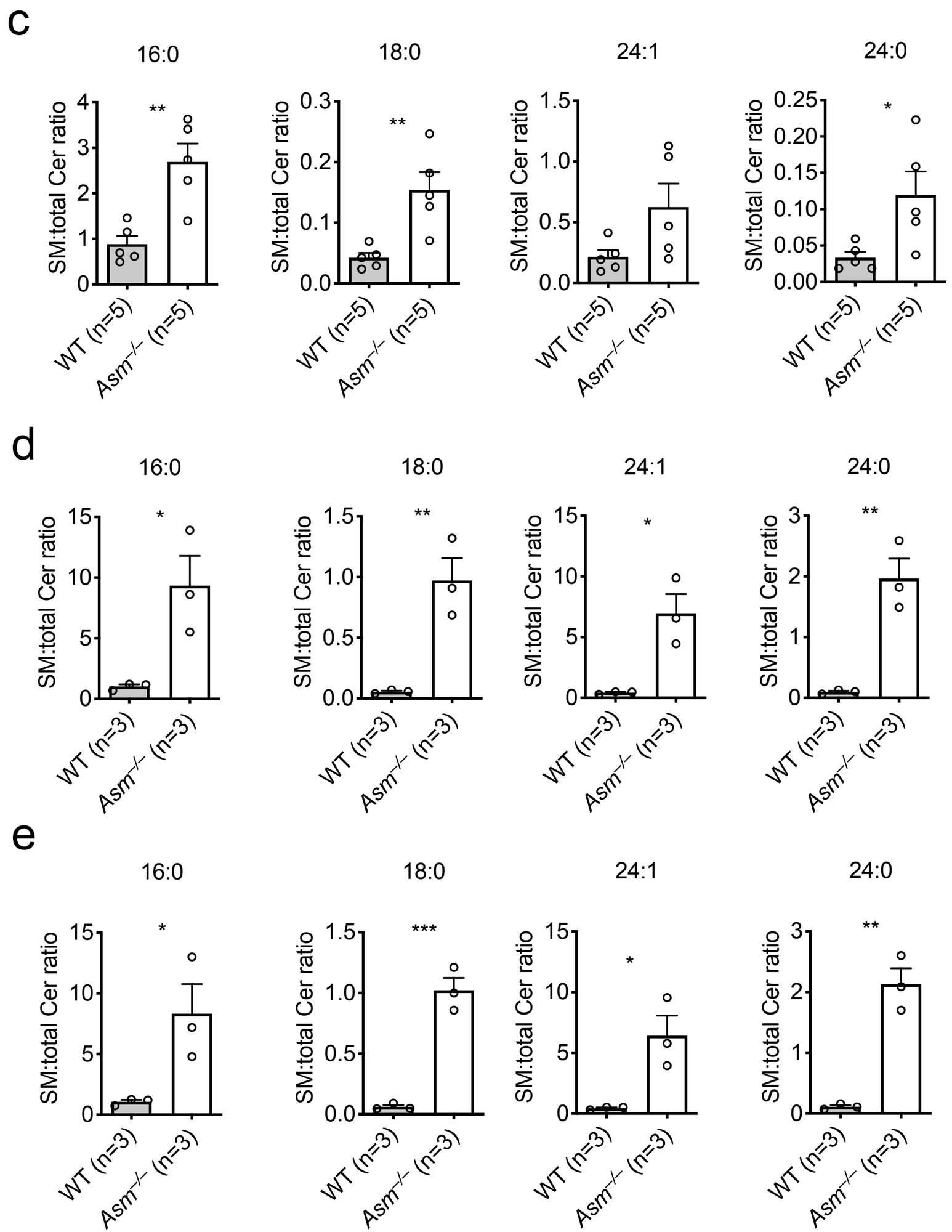
c
16:0
18:0
24:1
24:0
SM:total Cer ratio
WT (n=5)
Asm−/− (n=5)
d
16:0
18:0
24:1
24:0
SM:total Cer ratio
WT (n=3)
Asm−/− (n=3)
e
16:0
18:0
24:1
24:0
SM:total Cer ratio
WT (n=3)
Asm−/− (n=3)

# Figure 7

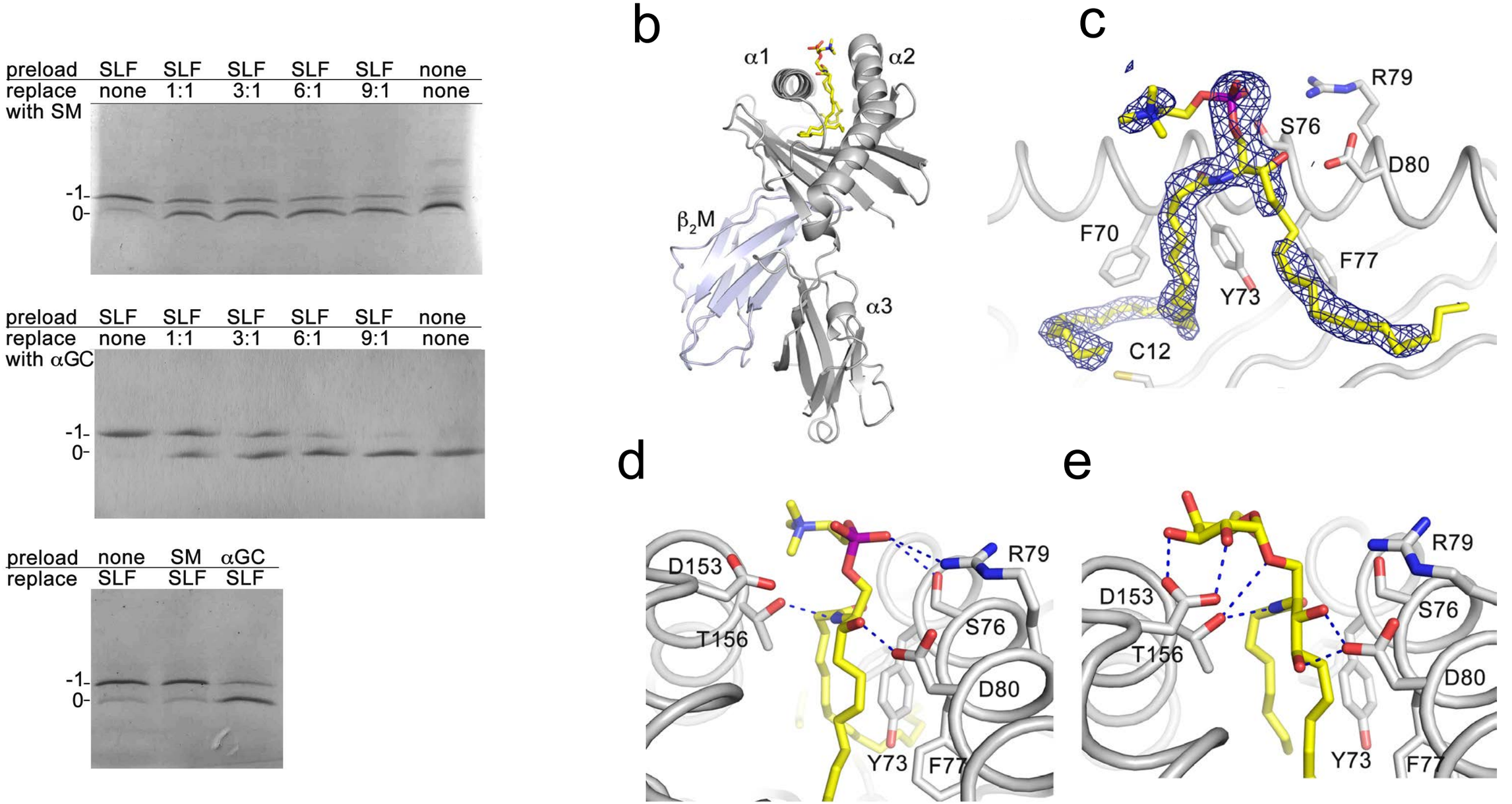
a
preload SLF SLF SLF SLF SLF none
replace none 1:1 3:1 6:1 9:1 none
with SM
-1-
0-
preload SLF SLF SLF SLF SLF none
replace none 1:1 3:1 6:1 9:1 none
with αGC
-1-
0-
preload none SM αGC
replace SLF SLF SLF
-1-
0-
b
α1
α2
β2M
α3
c
R79
S76
D80
F70
F77
Y73
C12
d
D153
R79
T156
S76
D80
Y73
F77
e
D153
R79
T156
S76
D80
Y73
F77

# Figure 8

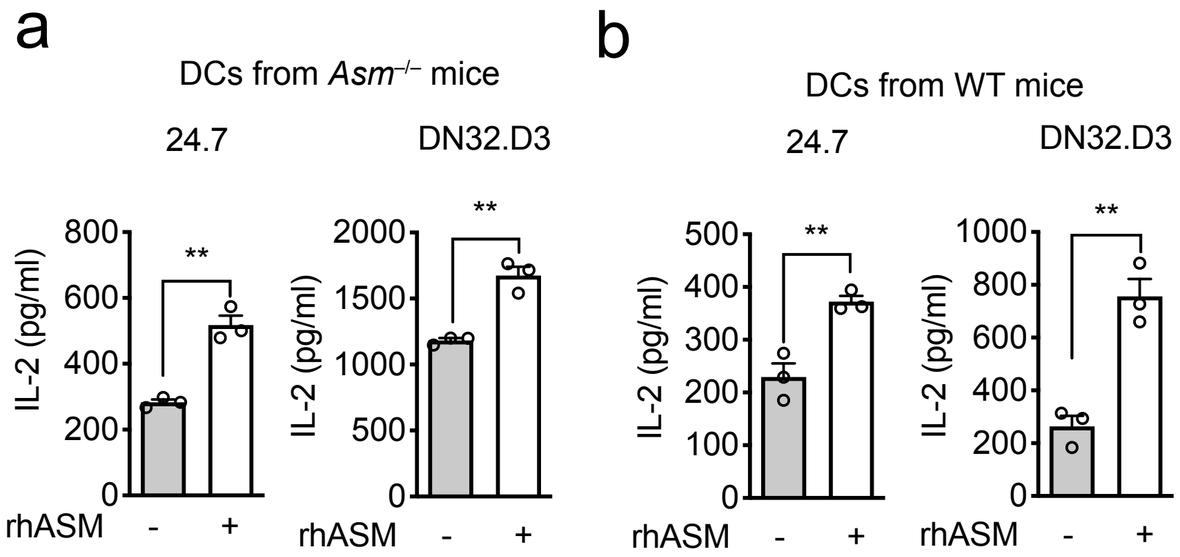
a
DCs from Asm−/− mice
24.7
DN32.D3
IL-2 (pg/ml)
rhASM
b
DCs from WT mice
24.7
DN32.D3
IL-2 (pg/ml)
rhASM

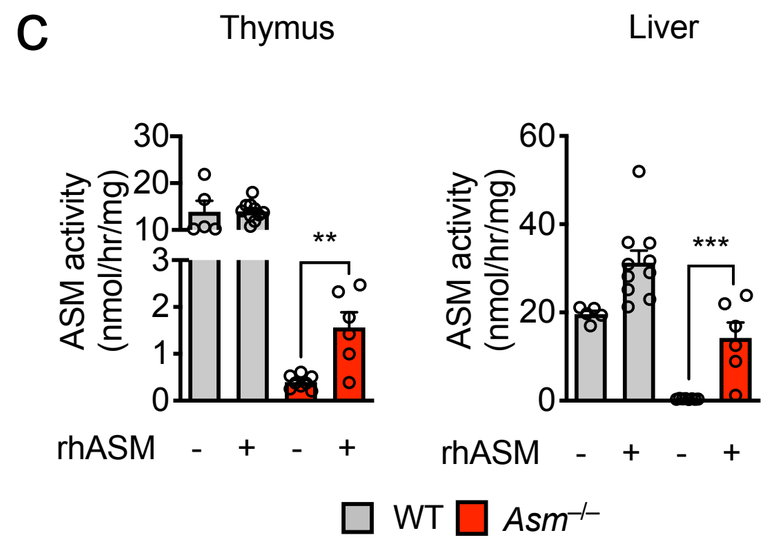
c
Thymus
Liver
ASM activity (nmol/hr/mg)
rhASM
WT
Asm−/−

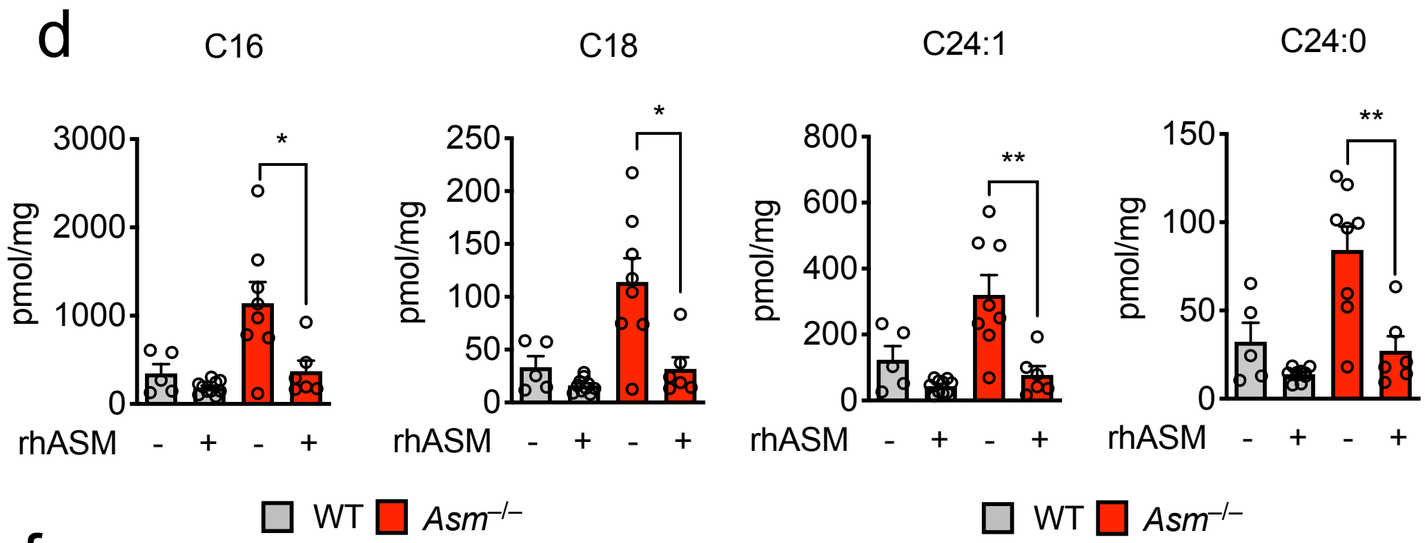
d
C16
C18
C24:1
C24:0
pmol/mg
rhASM
WT
Asm−/−

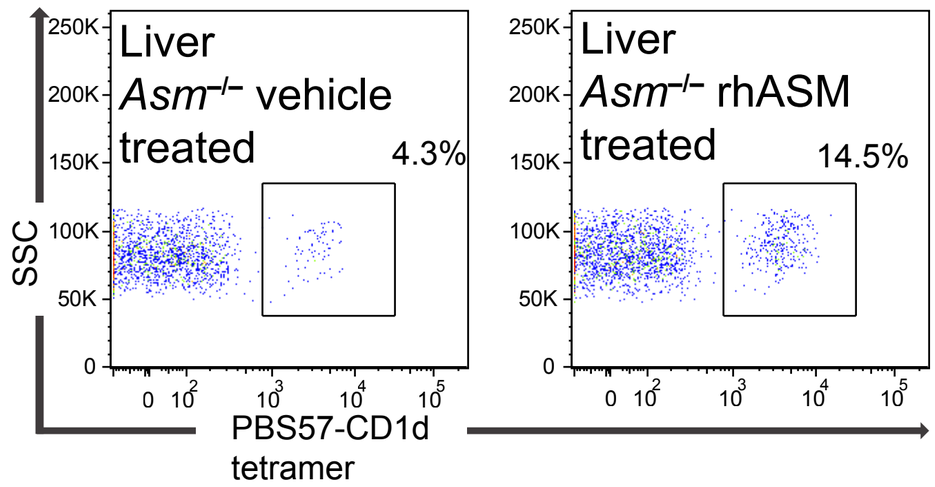
e
Liver
Asm−/− vehicle treated
4.3%
Liver
Asm−/− rhASM treated
14.5%
SSC
PBS57-CD1d tetramer

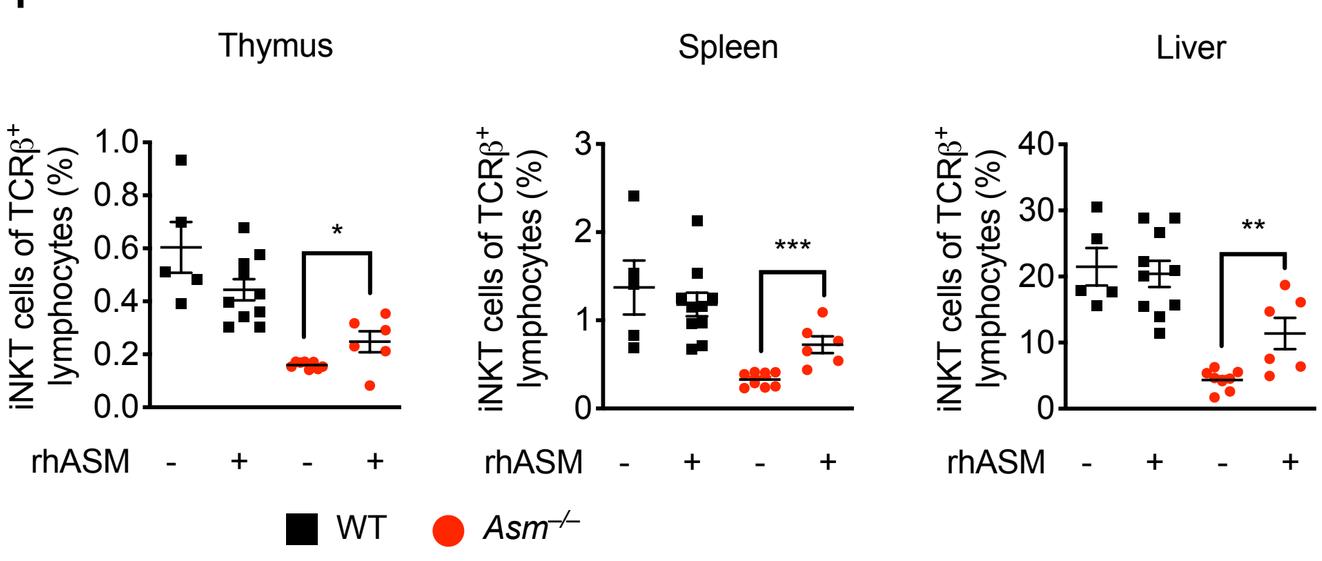
f
Thymus
Spleen
Liver
iNKT cells of TCRβ+ lymphocytes (%)
rhASM
WT
Asm−/−

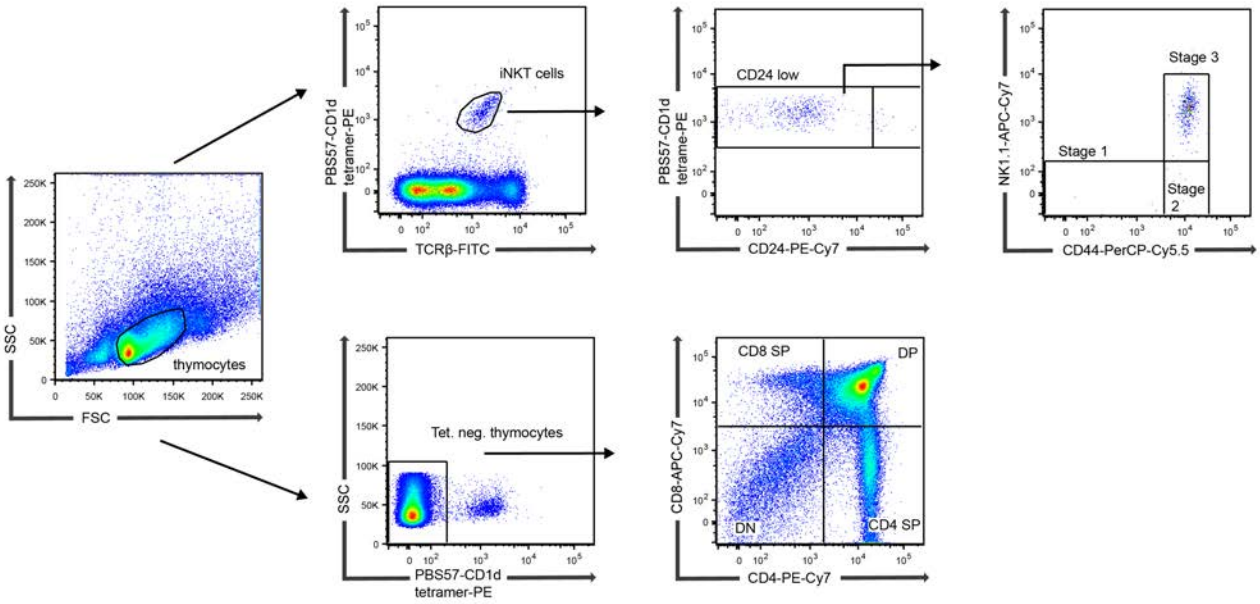


**Supplementary Figure 1**

**Examples of gating strategies for thymic samples.**

Thymocytes were prepared from the thymus and stained with monoclonal antibodies. The figure demonstrates representative dot plots and gating strategies for iNKT cells, iNKT cell stages, tetramer negative thymocytes and CD4/CD8 distribution. Other samples analyzed in the project were gated in a similar manner. SP single positive; DN double negative; DP double positive.

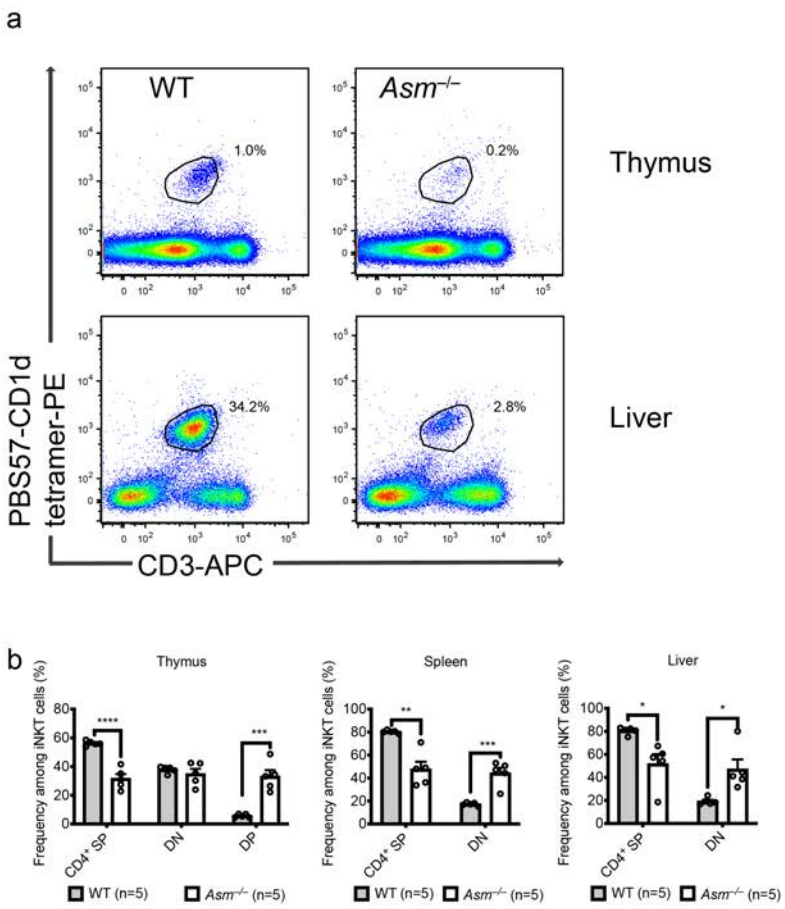


**Supplementary Figure 2**

**Acid sphingomyelinase deficient mice have reduced numbers of iNKT cells with an altered CD4/CD8 distribution.**

Lymphocytes were prepared from the tissues indicated in the figure followed by staining with monoclonal antibodies and a CD1d tetramer. (a) Representative flow cytometry dot plots of lymphocytes from WT and *Asm*$^{-/-}$ mice visualizing the number of iNKT cells in thymus and liver as defined by a PBS57-loaded CD1d tetramer and CD3. The results are representative of three independent experiments. (b) Distribution of CD4 and CD8 expression among iNKT cells from *Asm*$^{-/-}$(n=5) and WT (n=5) mice. The results are representative of two independent experiments. In all panels the mean values are shown with the error bars representing the SEM. *P*-values were calculated by two-sided t-test. **P*<0.05, ***P*<0.01, ****P*<0.001, *****P*<0.0001, SP single positive; DN double negative; DP double positive.

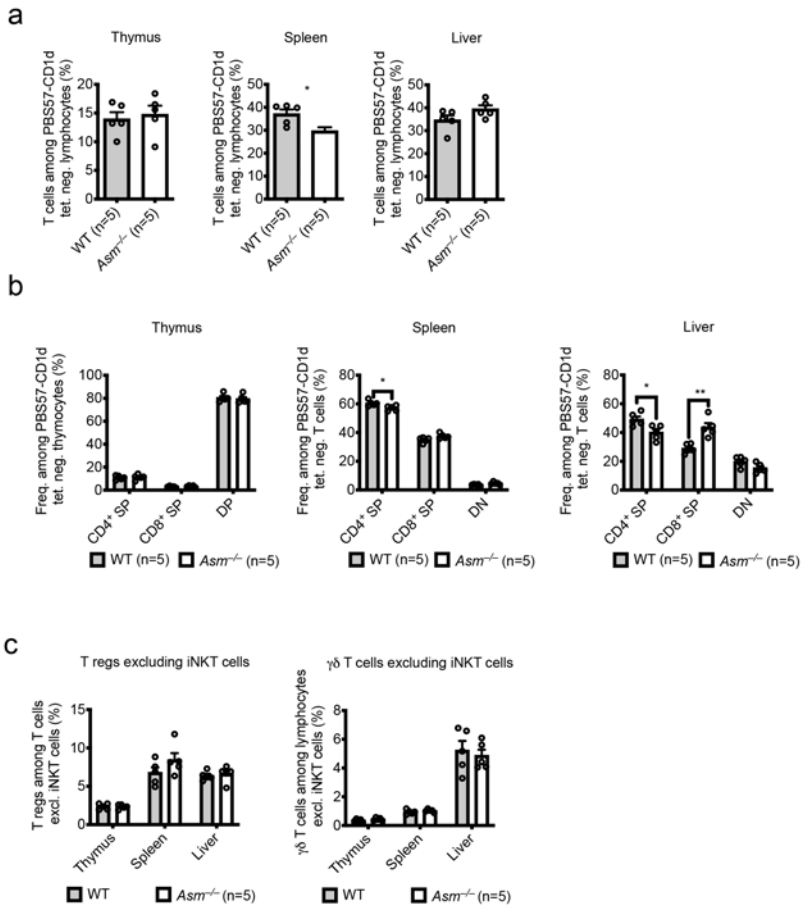


**Supplementary Figure 3**

**T cell distribution, CD4/CD8 expression, T regulatory cells and γδ T cells in *Asm*$^{-/-}$ compared to wildtype mice**

Lymphocytes were prepared from the indicated tissues from *Asm*$^{-/-}$ (n=5) and WT (n=5) mice and stained with monoclonal antibodies. (a) The percentages indicate CD3 positive cells among PBS57-CD1d tetramer negative lymphocytes. The results are representative of two independent experiments. (b) The percentages indicate the distribution of CD4 and CD8 expression among PBS57-CD1d tetramer negative thymocytes (for thymus) and PBS57-CD1d tetramer negative T cells (for spleen and liver). The results are representative of two independent experiments. (c) The percentages indicate the percentage of T regulatory cells or γδ T cells among T cells or lymphocytes excluding iNKT cells. The results are representative of two independent experiments. In all panels the mean values are shown with the error bars representing the SEM. *P*-values were calculated by two-sided t-test. **P*<0.05, ***P*<0.01, SP single positive; DN double negative; DP double positive.

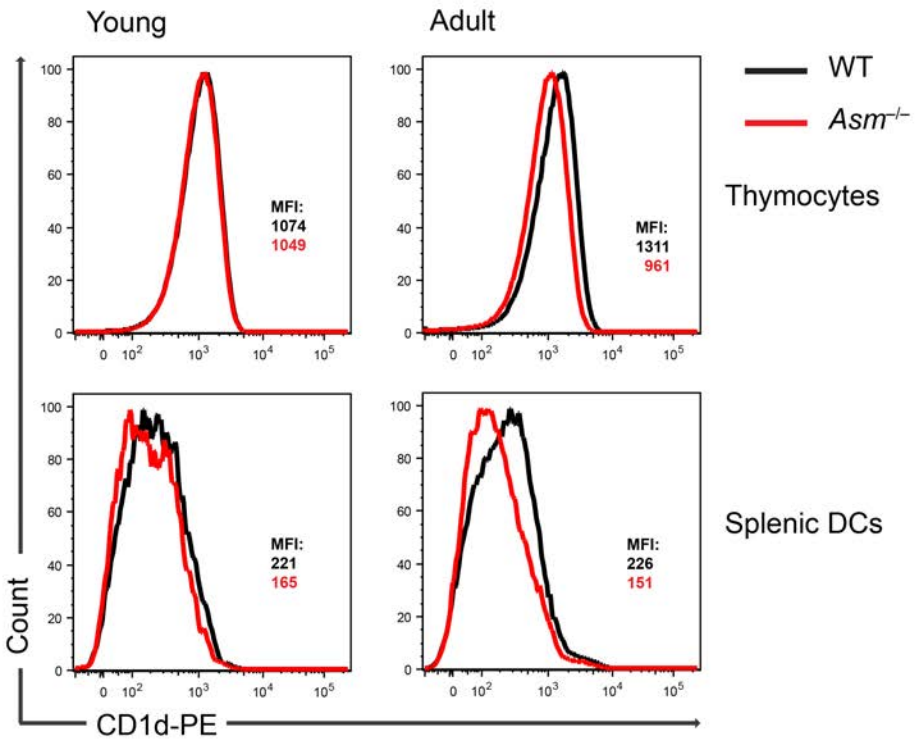


**Supplementary Figure 4**

**CD1d expression in thymocytes and CD11c$^+$ DCs from *Asm*$^{-/-}$ and wildtype mice.**

Thymocytes were prepared by manual maceration through a mesh and thereafter stained with a monoclonal antibody against CD1d. CD11c$^+$ DCs were extracted from spleens with CD11c magnetic beads and stained with a monoclonal antibody against CD1d. The two top histograms demonstrate the CD1d levels in thymocytes from young (left) and adult (right) mice. The two lower histograms demonstrate the CD1d levels in DCs from young (left) and adult (right) mice. The results are representative of three independent experiments. MFI median fluorescence intensity.

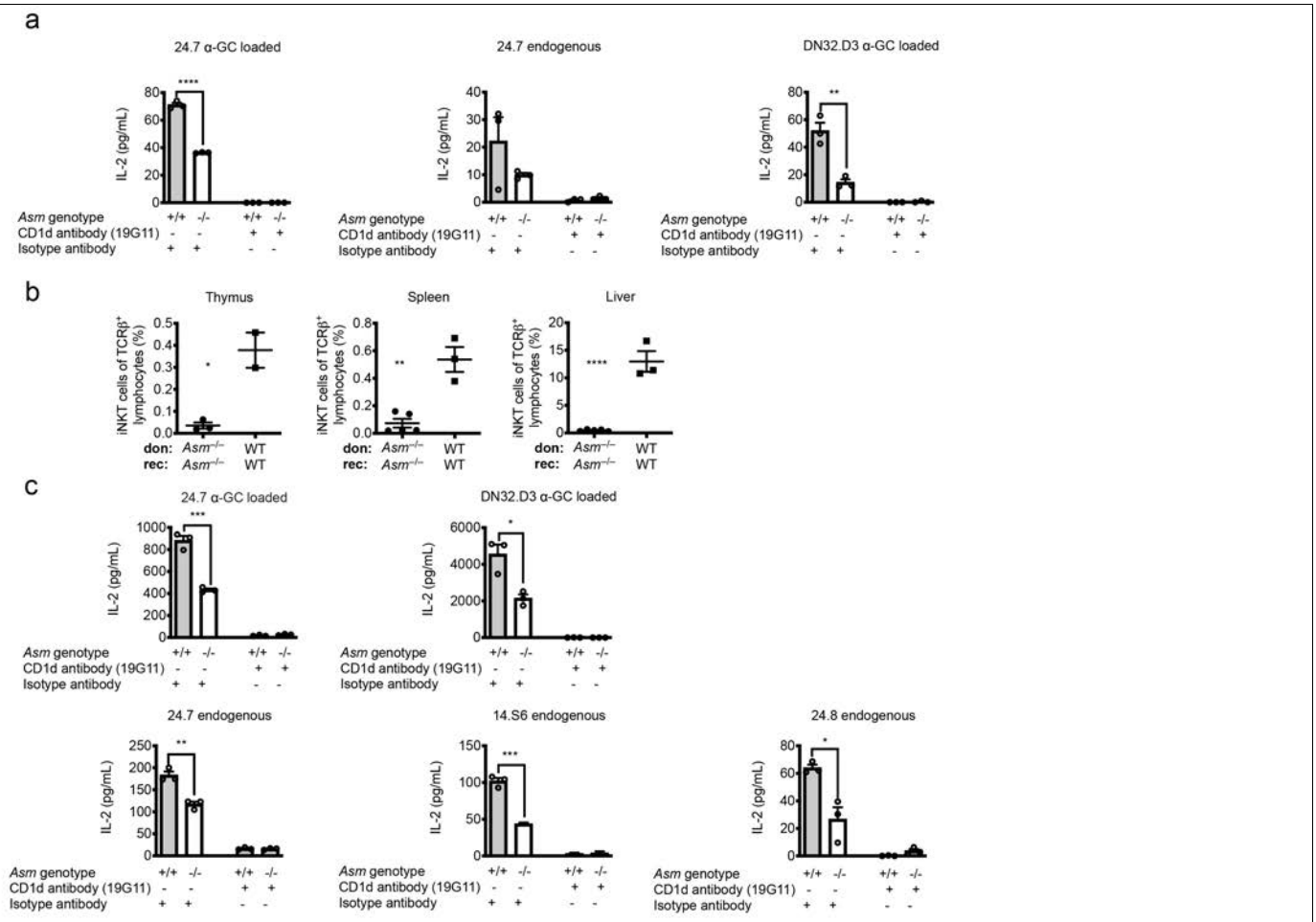


**Supplementary Figure 5**

**Activation of NKT cells by thymocytes and DCs is blocked by a CD1d antibody and bone-marrow transplantation in *Asm*$^{-/-}$ and wildtype mice.**

(a) Thymocytes were prepared by manual maceration through a mesh and loaded with α-GalCer for 4 hours (for 24.7 and DN32.D3 α-GC loaded) or left untreated (for 24.7 endogenous) followed by culture with the indicated NKT hybridomas for 16-24h. Cytokine levels were measured in the culture supernatants from three independent wells. The results are representative of two independent experiments. (b) Bone-marrow transplantation in *Asm*$^{-/-}$ (n=5) and WT mice (n=3). Bone-marrow chimeras were made by irradiating *Asm*$^{-/-}$ and WT mice followed by injection of donor bone-marrow from *Asm*$^{-/-}$ or WT mice. 3 months later the mice were sacrificed followed by flow-cytometry of tissue samples. The graphs demonstrate the percentage of CD1d-PBS57 tetramer positive cells among TCR-β positive cells (iNKT cells) from the indicated tissues. (c) CD11c$^{+}$ DCs were extracted from spleens with CD11c magnetic beads and loaded with α-GalCer for 4 hours (upper panel) or left untreated (lower panel) followed by co-culture with the indicated NKT hybridomas for 16-24h. Cytokine levels were measured in the culture supernatants from three independent wells. The results are representative of two independent experiments. In all panels the mean values are shown with the error bars representing the SEM. *P*-values were calculated by two-sided t-test. **P*<0.05, ***P*<0.01, ****P*<0.001, *****P*<0.0001

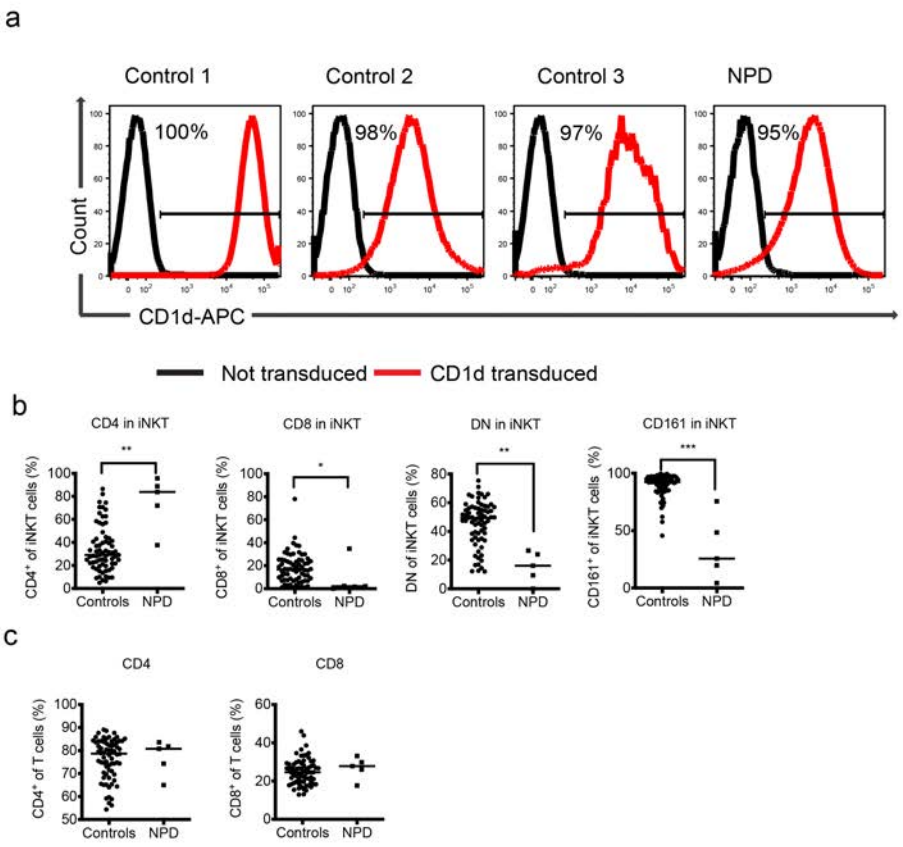


**Supplementary Figure 6**

**Transduction efficacy in transduced EBV transformed B-cells and Phenotype of iNKT cells and T cells in Niemann-Pick disease patients compared to controls**.

(a) EBV transformed B-cells from three healthy controls and one Niemann-Pick disease (NPD) patient were lentivirally transduced with a construct encoding human CD1d. The cells were thereafter subjected to FACS sorting. The histograms indicate the CD1d expression in the transduced and sorted cells (red lines) compared with the corresponding untransduced cells (black line). (b,c) Phenotype of iNKT cells and T cells in NPD patients compared to controls. Lymphocytes from five NPD patients (four type B and one type A) and 70 healthy controls were investigated with flow-cytometry. (b) CD4, CD8, double negative (DN) and CD161 distribution in iNKT cells. (c) CD4 and CD8 distribution in T cells. The line indicates the median. A two-sided Mann-Whitney test was used for significance testing. *$P$<0.05, **$P$<0.001 ***$P$<0.0001. NPD Niemann-Pick disease; DN double negative.

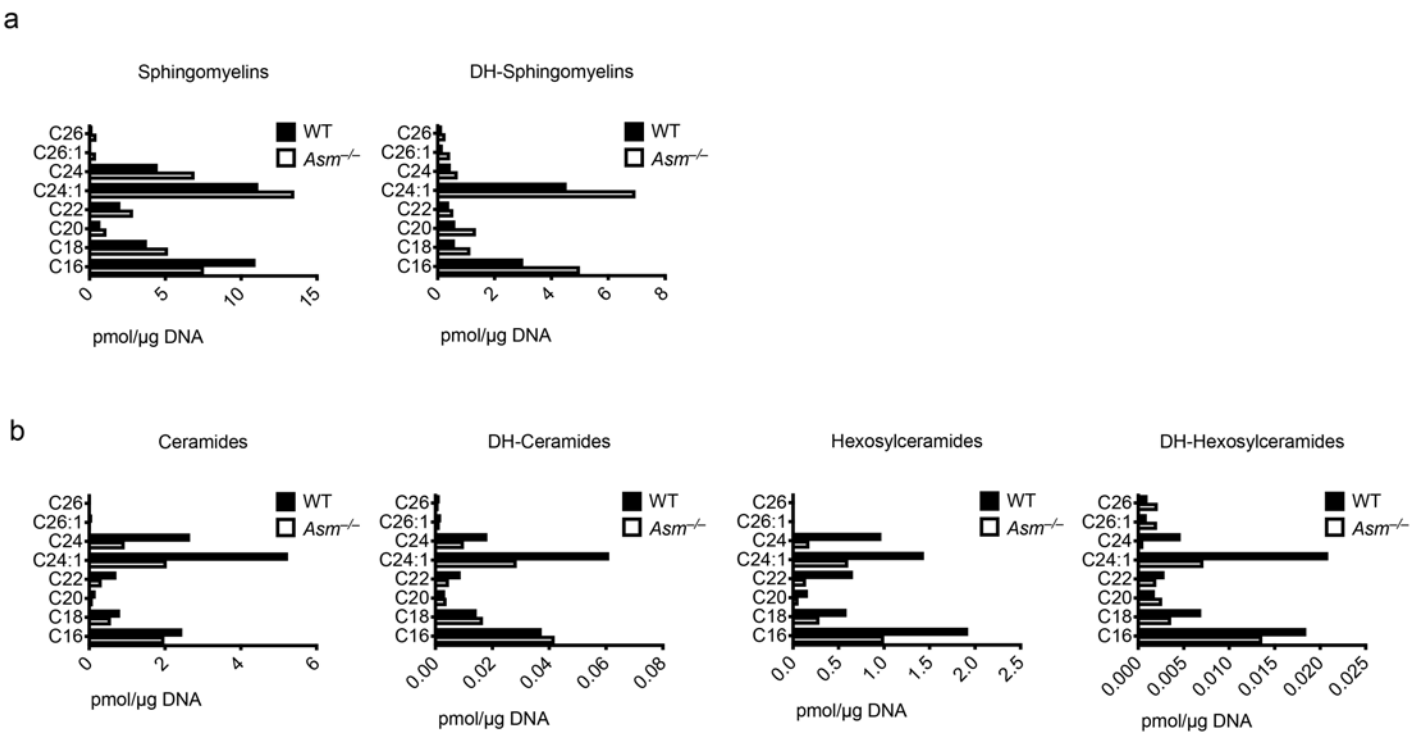


**Supplementary Figure 7**

**Lipidomics results from liver samples from 2 week old *Asm*$^{-/-}$ and wildtype mice.**

Sphingomyelin and ceramide levels in the liver of 2 week old *Asm*$^{-/-}$ (n=2) and wildtype (n=2) mice were quantified by mass spectrometry. (a) The graphs show the mean levels of sphingomyelins and DH-sphingomyelins with carbon chains of different lengths. (b) The graphs show the mean levels of ceramides, DH-ceramides,hexosylceramides and DH-hexosylceramides with carbon chains of different lengths.

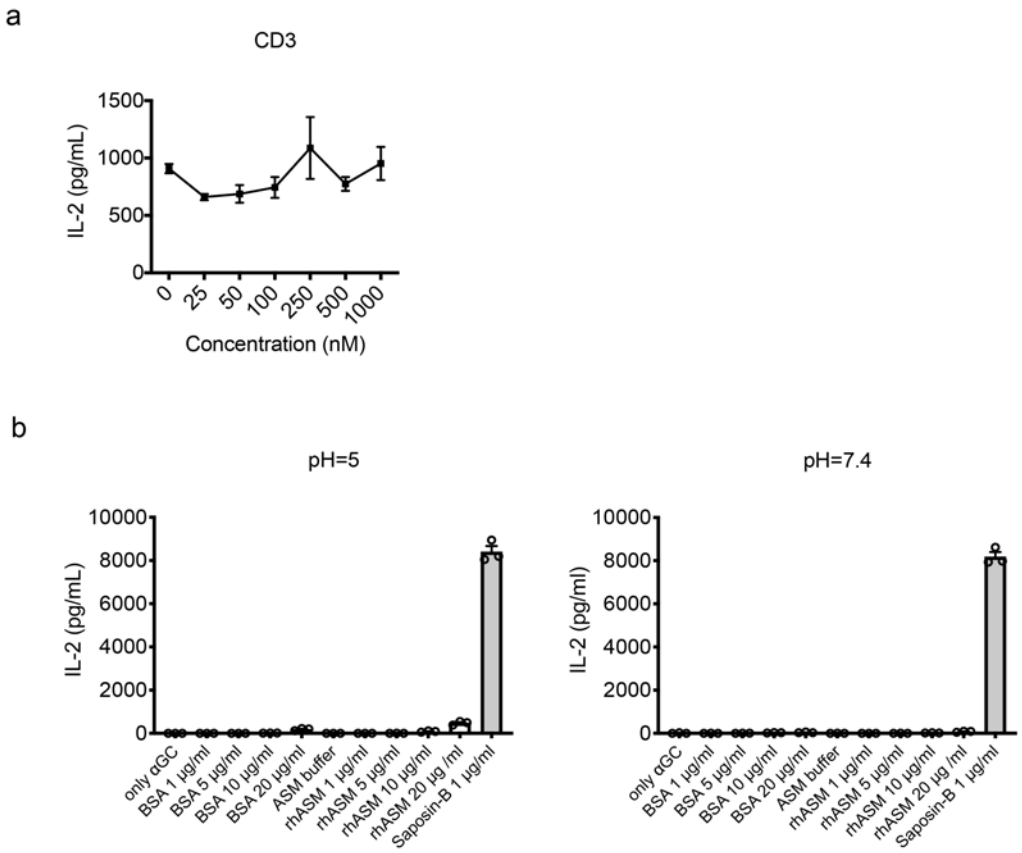


**Supplementary Figure 8**

**Sphingomyelin does not affect direct activation of iNKT cells and acid sphingomyelinase does not directly affect loading of lipid antigens.**

(a) Cell-culture plates were first coated with CD3 followed by incubation with the indicated concentrations of sphingomyelin 24:1. After thorough washing the DN32.D3 hybridoma was added and incubated for 16 hours. IL-2 levels in the supernatant were determined by ELISA. The results are representative of two independent experiments. (b) Murine CD1d was coated on cell-culture plates followed by incubation with α-GalCer and Saposin-B, rhASM or BSA in the indicated concentrations overnight. Thereafter, the DN32.D3 hybridoma was added for 16 hours. IL-2 levels in the supernatant were determined by ELISA. The left panel shows the results when the experiment was performed under acidic conditions while the right panel show the results under neutral conditions. The results are representative of two independent experiments. In all panels the mean values are shown with the error bars representing the SEM.

| Patient number | Disease | Sex | Age (years) | Sphingomyelinase activity in patient fibroblasts * |
|---|---|---|---|---|
| 1 | NPD A | M | 1 | not available |
| 2 | NPD B | M | 41 | not available |
| 3 | NPD B | M | 54 | 2.06 nmol/h/mg |
| 4 | NPD B | F | 10 | 0.2 nmol/h/mg |
| 5 | NPD B | F | 41 | not available |

**Suppl. Table 1.** Clinical information on NPD patients analyzed for NKT-cells.
*reference values for control subjects between 84 and 285